

AD-A115 483

AIR FORCE INST OF TECH WRIGHT-PATTERSON AFB OH SCH00--ETC F/6 12/1

SMOOTH FIT ANALYSIS OF MOESSBAUER SPECTRA.(U)

MAR 82 T L BAZZOLI

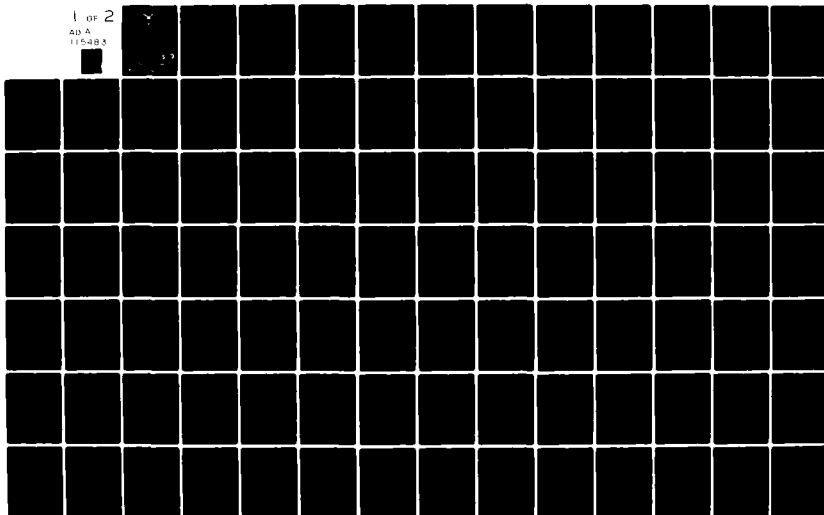
UNCLASSIFIED

AFIT/GNE/PH/82-2

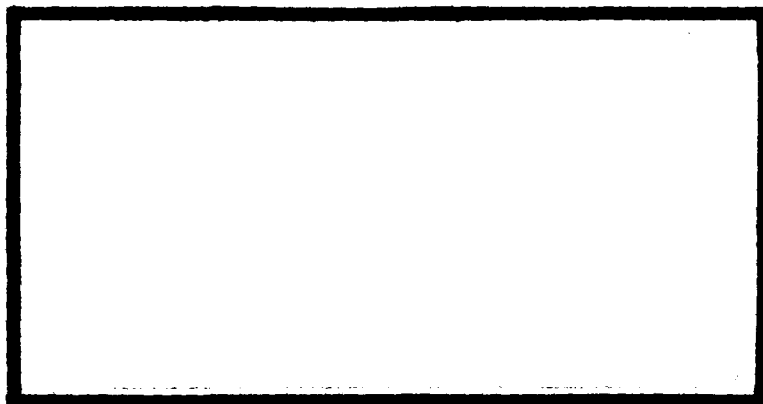
NL

1 OF 2

AD A
115483



AD A115483



DTIC FILE COPY

DEPARTMENT OF THE AIR FORCE
AIR UNIVERSITY (ATC)
AIR FORCE INSTITUTE OF TECHNOLOGY

Wright-Patterson Air Force Base, Ohio

This document has been approved
for public release and sale; its
distribution is unlimited.

82 06 14 190

DTIC
ELECTE
JUN 14 1982
S D
E

AFIT/GNE/PH/82-2

①

SMOOTH FIT ANALYSIS OF
MÖSSBAUER SPECTRA

THESIS

AFIT/GNE/PH/82-2

Thomas L. Bazzoli
Lieutenant USAF

RECEIVED
AFIT/GNE/PH/82-2
E

Approved for public release; distribution unlimited.

SMOOTH FIT ANALYSIS OF
MÖSSBAUER SPECTRA

THESIS

Presented to the Faculty of the School of Engineering
of the Air Force Institute of Technology

Air University
in Partial Fulfillment of the
Requirements for the Degree of
Master of Science

by
Thomas L. Bazzoli, B.S. Chemistry
Lieutenant USAF

Graduate Nuclear Effects

March 1982

Accession For	
NTIS GRA&I	<input checked="checked" type="checkbox"/>
DTIC TAB	<input type="checkbox"/>
Unannounced	<input type="checkbox"/>
Justification	
By _____	
Distribution/	
Availability Codes	
Dist	Avail and/or Special
A	



Approved for public release; distribution unlimited.

Acknowledgments

I would like to thank and acknowledge my advisor, Dr. Donn Shankland for suggesting this project and for pointing me in the right direction when I had wandered off on my own tangents. I would also like to extend special thanks to my classmates of GNE-82M who were eager to encourage me when my problems seemed insurmountable.

Contents

	Page
Acknowledgments	ii
List of Figures	v
List of Tables	vii
Abstract	viii
I. Introduction	1
Background	1
Method	4
Purpose	7
Overview	7
II. Development of Fitting Technique	8
Least-Squares Approach	8
Limitations on the Magnetic Field	
Density	10
Nonnegative	11
Smooth	11
Minimization	12
Numerical Solution for the Integral	16
Lineshape Function	16
Set of Functions ϕ_n	18
Integral Approximation	20
Recursion Relation	24
III. Computer Program Development	30
Computation of $r_n(c)$	30
Subroutine FIX	32
Subroutine CONS	33
Subroutine INTEG	35
Subroutine RITEO	36
Determination of $\rho(H)$	36
Subroutine READN	36
Subroutine MATR1	39
Subroutine HERMIT	39
Subroutine MESCHP	39
Subroutine MAGFD	40
Subroutine PLTMAG	40
Computation of Fit Spectrum	41
Subroutine SPCTRM	41
Subroutine PLTSPT	42

	Page
Other Routines	42
Subroutine CONST	42
Subroutine MATRN	43
IV. Program Validation	44
V. Results, Recommendations and Conclusions	59
Optimizing Results	59
Conclusions	60
Recommendations	62
Bibliography	64
Appendix A: Input Parameters for Program RPARAM	66
Appendix B: Computer Program Listings	70
Vita	99

List of Figures

Figure	Page
1 Magnetic Field Density and the Resulting Spectra from an Amorphous Material	2
2 Magnetic Field Density and the Resulting Spectra from an Alloy in the Crystalline State	3
3 Flow Diagram for RPARAM	31
4 Generalized Flowchart for MOSFIT pt. I	37
5 MOSFIT Flowchart pt. II	38
6 Examination of the General Lineshape Produced With Given Data	45
7 Magnetic Field Density Used to Generate Test Spectrum	49
8 Input Test Spectrum	50
9 Magnetic Field Density from Initial Test Run	52
10 Fit Spectrum from Numerical Integration in Initial Run	53
11 Magnetic Field Density With 2x Correction Factor	54
12 Fit Spectrum by Numerical Integration and 2x Factor	55
13 Fit Spectrum Using $r_n(c)$ Values Without 2x Factor	56
14 Fit Spectrum Using $r_n(c)$ Values and 2x Factor	57
15 Result Optimization	60
A-1 Relation of Input Parameters to Spectrum	66
A-2 Splitting of the Fe ⁵⁷ Nucleus	68

Figure	Page
B-1 Flowchart for Subroutine CONS	74
B-2 Flowchart for Subroutine INTEG	76
B-3 Flowchart for Subroutine COEFF	82
B-4 Continuation of COEFF Flowchart	83
B-5 Flowchart for Subroutine HERMIT	87
B-6 Flowchart for Subroutine MAGFD	89
B-7 Flowchart for Subroutine SPCTRM	94

List of Tables

Table		Page
I	Input Parameters for Fe ⁵⁷	32
II	Evaluation of FNJ	46

Abstract

A method of fitting the magnetic field distribution from Mössbauer spectra using a linear least-squares technique was proposed where the distribution was assumed to be an expansion in Hermite polynomials. This method was developed, programmed and tested on a test spectrum with a known distribution of magnetic field. The programming was not entirely successful in reproducing this test spectra and no actual data was analyzed to support the effectiveness of this method.

SMOOTH FIT ANALYSIS OF MÖSSBAUER SPECTRA

I. Introduction

Mössbauer spectroscopy is known for its applicability in many fields and, as a result, has become a valuable tool in most disciplines of science. Today, the principles involved in nuclear gamma-ray resonance spectroscopy are well documented in the literature (Ref 1,2). However, while a Mössbauer spectrum can provide a wealth of information on the properties of a material under investigation, much of this information can be lost in the statistical fluctuations of the data and the complexity of the spectrum. In response to the problems of Mössbauer analysis, many researchers have developed techniques of fitting Mössbauer spectra. This work examines a fitting procedure developed by Dr. Donn G. Shankland (Ref 3).

Background

A Mössbauer spectrum can provide a means to investigate the microscopic fields of a material. One class of materials that is of interest to the Air Force is amorphous metal alloys, which are known for their flexibility and high strength. The disorganized lattice structure of these alloys results in various magnetic fields from short range ordering (Ref 4). These fields are distributed in a

probability distribution commonly called the magnetic field density and represented as $\rho(H)$. In the amorphous state, this distribution is continuous and the resulting Mössbauer spectrum is broad without distinct peaks. An example of the distribution and spectrum expected from an amorphous material is shown in Figure 1.

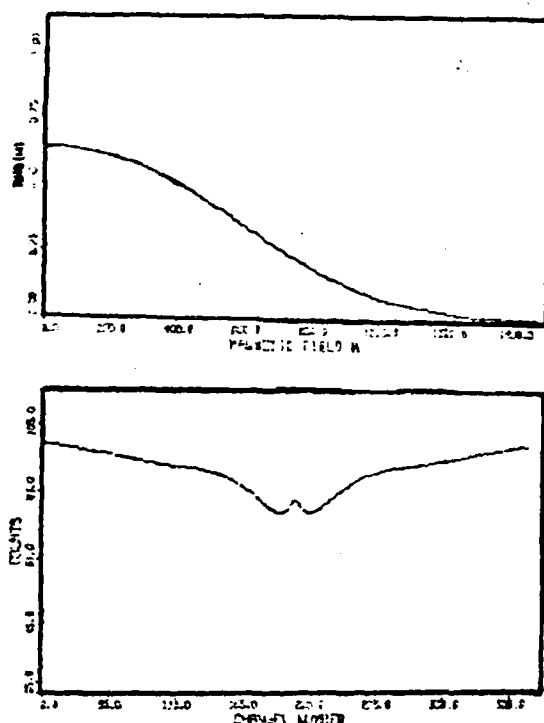


Figure 1. Magnetic Field Density and the Resulting Spectra from an Amorphous Material

On the other hand, as the amorphous alloy crystallizes, distinct magnetic domains will develop--each with a discrete magnetic field. The alloys of interest to the Air Force consist of various iron compounds. When Fe^{57} is present in

an absorber and a magnetic field exists, the resulting Mössbauer spectrum will consist of six peaks that correspond to the six allowed transitions in this isotope. Each discrete magnetic field will cause this spread of the Mössbauer lines. As a result, the Mössbauer spectrum of the crystalline state will consist of a set of overlapping six peak spectra, each set corresponding to a discrete magnetic field. A conceptual representation of the magnetic field density and spectrum of the crystalline alloy is found in Figure 2.

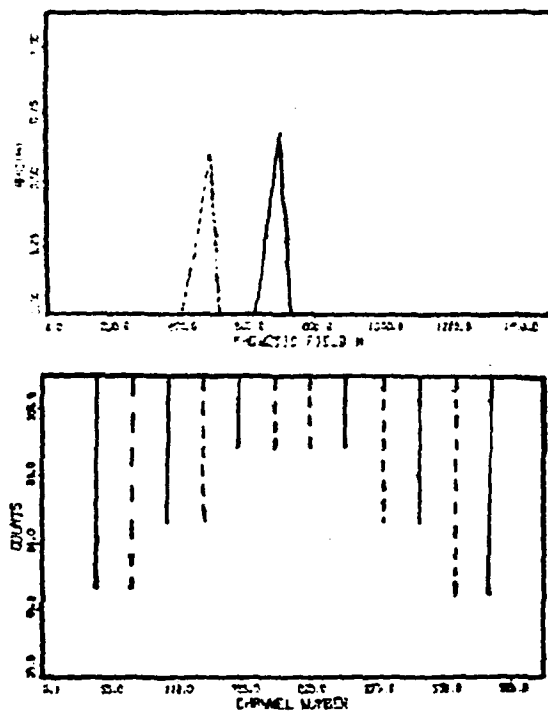


Figure 2. Magnetic Field Density and the Resulting Spectra from an Alloy in the Crystalline State

This study investigates a method for finding the magnetic field density from amorphous metal alloys and using the result in a fit of the Mössbauer spectrum.

Method

The data collected in the investigation of the Mössbauer effect is generally in the form of a digitized spectrum that represents the interaction of gamma radiation with a given detector. Since random processes are involved in radioactive decay, absorption, reemission and detection, the individual data points are subject to a degree of statistical fluctuation. The predominant method of minimizing this statistical error involves the application of a least-squares fitting technique.

In general, least-squares fitting requires the comparison of the data with a functional approximation of this data. The approximating function should be chosen so that the sum of the squares of the difference between the data and this function is minimized. That is, if the data is represented as n_i and the functional approximation is $n(c)$, then the expression

$$S = \sum (n_i - n(c))^2$$

is minimized. This minimization is accomplished by determining the parameters in $n(c)$ which can be varied, and then, the partial derivatives of S with respect to each of these parameters are found and set equal to zero.

The preliminary task in performing the least-squares fitting is to develop the approximating function or theoretical model to describe the data obtained. This model is used to represent the expected or "true" values to be compared with the experimental data in the analysis. When a multichannel analyzer is used to collect a Mössbauer spectrum, then the number of counts in channel c , $n(c)$, is found by

$$n(c) = n_B(c) - \int_0^\infty dH \rho(H) L(c, H)$$

where $n_B(c)$ is the number of background counts in channel c , H is the magnetic field strength, $\rho(H)$ is the aforementioned magnetic field density, and $L(c, H)$ is a function representing the lineshape of the spectral peaks (Ref 4).

However, problems tend to arise in the evaluation of this function. The approximating equation is a Fredholm integral function of the first kind and problems occur when the integral is approximated numerically (Ref 5). The solution of this integral is nonunique and the problem becomes ill-posed since the solution process is highly sensitive to the data. As a result, it is advantageous to find an analytical solution to this problem by choosing the appropriate functional forms of $L(c, H)$ and $\rho(H)$.

Since Fe^{57} is the absorber in the amorphous metal alloys, it can be assumed that the spectrum of the alloy will be fundamentally related to the six peak spectrum of

Fe^{57} in the presence of a magnetic field. Therefore, the overall lineshape function can be represented as the sum of six individual peak shapes. Most work in Mössbauer spectroscopy describes individual absorption peaks with a simple Lorentzian formula. In contrast, this work describes the lineshape as a sum of six Gaussian peaks in order to facilitate the analytical solution of the integral.

In the simplification of the integral, other investigators have assumed a shape, or modelled the magnetic field density in their attempts to fit Mössbauer spectra (Ref 6-10). Shankland chose to fit $\rho(H)$ by an expansion in Hermite polynomials. Combining this fit of the magnetic field density with the lineshape function reduces the integral can be approximated by a given number of series terms. The solution is developed so that the number of series terms chosen will correspond to the number of Hermites in the expansion of $\rho(H)$. The integral terms are incorporated in a matrix minimization problem in the least-squares analysis. The solution of the minimization problem will yield a magnetic field distribution that is continuous and best represents the microscopic field distribution that produced the data.

Two problems may arise in this approach. If a sharp peak (or peaks) occurs in the magnetic field density, a large number of polynomials will be required to reproduce the peak. Therefore, errors can be introduced when only a

few Hermite polynomials are used in the expansion of $\rho(H)$. In addition, the $\rho(H)$ generated may consist of nonphysical negative values. This requires the addition of the constraint that the magnetic field always be positive. This study attempts to fit Mössbauer spectra by representing $\rho(H)$ as an expansion of Hermite polynomials.

Purpose

The purpose of this study was to investigate the effectiveness of using Dr. Shankland's method for fitting $\rho(H)$ and subsequently using the result to determine the fit spectrum. Implementation of this method involved writing two computer codes using the numerical procedure developed, validating the method by generating a test spectrum with known $\rho(H)$ and then applying the method to actual Mössbauer data.

Overview

The theory of Mössbauer spectroscopy is well known and will not be discussed (Ref 1,2). Chapter II contains a detailed development of Dr. Shankland's fitting procedure. The implementation of this theory is discussed with the development of the computer codes in Chapter III. Chapter IV describes the procedures used in the validation and testing of the programs. The final chapter includes the results, conclusions and recommendations.

II. Development of Fitting Technique

In the measurement of the Mössbauer effect, a digital spectrum consisting of background counts and a number of absorption peaks is produced. This digitized data results from gamma ray emission, absorption and detection. Consequently, these measurements, or counts in the experimental sense, are subject to inherent statistical fluctuation that introduces uncertainty into the results. In order to investigate the microscopic fields of amorphous metal alloys, the magnetic field distribution that produces this data must be found. Dr. Shankland has developed a method of fitting the magnetic field distribution of Mössbauer spectra by employing a linear least-squares technique.

Least-Squares Approach

Since the experimental data, n_i , is subject to the errors of counting statistics, it is desirable to find a "best fit" of the data with respect to the "true" or expected results. A common means of curve fitting is the method of least-squares (Ref 11). In general, a least-squares fit chooses certain parameters to minimize the relation

$$\sum_i w_i v_i^2 \quad (2.1)$$

where

w_i represents a weighting factor

v_i is the residual or difference between the true
and observed results

When a multichannel analyzer is used to collect the Mössbauer spectra, the "true" results, $n(c)$, can be predicted by the approximating function

$$n(c) = n_B(c) - \int_0^\infty dH \rho(H) L(c, H) \quad (2.2)$$

where

$n_B(c)$ is the number of background counts in
channel c

$\rho(H)$ is the magnetic field density from all sources

$L(c, H)$ is a lineshape function used to describe the
absorption peaks in the spectrum

With the residual, $v_i = n(c) - n_i$, Eq (2.1) becomes

$$\sum_i w_i (n(c) - n_i)^2 \quad (2.3a)$$

or

$$\sum_i w_i [n_i - n_B(c_i) + \int_0^\infty dH \rho(H) L(c_i, H)]^2 \quad (2.3b)$$

In counting statistics, errors are found to vary like

$\sigma_i \approx \sqrt{n_i}$ (Ref 12). If the error is examined as a fraction of the individual data, $\sqrt{n_i}/n_i$, it is evident that this fractional error can be found to vary as $\sigma'_i = \frac{1}{\sqrt{n_i}}$.

Since σ_i^2 is a measure of the expected deviation from the true value for a given data point, it would be reasonable to minimize the residual weighted by $\frac{1}{\sigma_i^2}$ (Ref 11). Hence, the least squares relation is

$$S_o = \frac{1}{2} \sum_i n_i [n_i - n_B(c) + \int_0^\infty dH \rho(H) L(c, H)]^2 \quad (2.4)$$

where the $\frac{1}{2}$ is a constant of proportionality. Finally, the background $n_B(c)$ must be described. Since the background is diffuse and is assumed to be curved, it can be adequately modelled by a quadratic of the form

$$n_B(c) = b_0 + b_1 c + b_2 c^2 \quad (2.5a)$$

or

$$n_B(c) = \sum_{\gamma=0}^2 b_\gamma c^\gamma \quad (2.5b)$$

Thus, Eq (2.4) becomes

$$S_o = \frac{1}{2} \sum_i n_i [n_i - \sum_\gamma b_\gamma c^\gamma + \int_0^\infty dH \rho(H) L(c, H)]^2 \quad (2.6)$$

which is the system to be minimized.

Limitations on the Magnetic Field Density

It is also desired that this fit be subject to the criteria that the magnetic field density, $\rho(H)$, be smooth and nonnegative. The fit must be subject to these conditions because the smoothness of the fit spectra is directly

related to the smoothness of $\rho(H)$. In addition, it is important to eliminate nonphysical negative values of the distribution.

Nonnegative. Generally, there may be one or more of the discrete points H_α where $\rho(H_\alpha)$ will solve as negative. These points must be constrained to zero to fulfill the condition that $\rho(H)$, which represents a probability distribution of magnetic field strengths, be positive or zero. With the addition of constraints

$$S_c = \frac{1}{2} \sum_i n_i [n_i - \sum_\gamma b_\gamma c^\gamma + \int_0^\infty dH \rho(H) L(c, H)]^2 - \sum_q \lambda_q \rho(H_{\alpha_q}) \quad (2.7)$$

where

$\rho(H_{\alpha_q})$ are the negative values of $\rho(H_\alpha)$

λ_q are the Lagrangian multipliers for each constrained point

Smooth. The roughness of $\rho(H)$ could be measured by a quadratic form in $\rho(H)$ and its various derivatives. Therefore, a smoothing function can be represented as

$$R_0 = \int_0^\infty dH \rho(H) g\left(\frac{-d^2}{dH^2}\right) \rho(H) \quad (2.8)$$

with $g\left(\frac{-d^2}{dH^2}\right)$ as an operator in the derivatives of $\rho(H)$.

However, the appropriate operator is dependent on the functional form of the magnetic field density. As a result, it is desirable to represent the smoothness function as

$$R_o = \int_0^\infty dH \rho(H) g(-\Delta^2) \rho(H) \quad (2.9)$$

where the $g(-\Delta^2)$ represents any operator that will provide a measure of roughness for the specific form of $\rho(H)$.

The R_o term in Eq (2.9) is weighted and added to the system so that it may be minimized simultaneously with the constrained data error S_c . That is,

$$S = \alpha S_c + \beta R_o \quad (2.10)$$

If the weight terms are chosen such that $\alpha = 1$ and $\beta = \frac{A}{2}$, the system to be minimized becomes

$$S = \frac{1}{2} \sum_i n_i [n_i - \sum_\gamma b_\gamma c_i^\gamma + \int_0^\infty dH \rho(H) L(c_i, H)]^2 \\ - \sum_q \lambda_q \rho(H_{\alpha_q}) + \frac{A}{2} \int_0^\infty dH \rho(H) g(-\Delta^2) \rho(H) \quad (2.11)$$

Minimization

In order to compute the "best" smooth-fit of the experimental data, Eq (2.11) must be minimized with respect to the parameters $\rho(H)$, b_γ , and λ_q . Thus, on differentiation,

$$\frac{\partial S}{\partial \rho(H)} = 0 = \sum_i n_i [n_i - \sum_\gamma b_\gamma c_i^\gamma + \int_0^\infty dH' \rho(H') L(c_i, H') L(c_i, H) - \lambda_q \delta(H-H_q) + Ag(-\Delta^2) \rho(H)] \quad (2.12a)$$

$$\frac{\partial S}{\partial \rho(H)} = 0 = \sum_i n_i [n_i - \sum_\gamma b_\gamma c_i^\gamma + \int_0^\infty dH' \rho(H') L(c_i, H')] (-c_i^\gamma) \quad (2.12b)$$

$$\frac{\partial S}{\partial \lambda_q} = 0 = -\rho(H_q) \quad (2.12c)$$

where $\delta(H-H_q)$ in Eq (2.12a) represents a Dirac delta function at H_q . With rearrangement, the three equations in Eq (2.12) yield

$$\begin{aligned} \int dH' [\sum_i n_i L(c_i, H) L(c_i, H')] \rho(H') + Ag(-\Delta^2) (H') \\ - \sum_\gamma [\sum_i n_i L(c_i, H) c_i^\gamma] b_\gamma - \lambda_q \delta(H-H_q) \\ - \sum_i n_i^2 L(c_i, H) = 0 \end{aligned} \quad (2.13a)$$

$$\begin{aligned} \int dH' [\sum_i n_i c_i^\gamma L(c_i, H')] \rho(H') + \sum_{\gamma'} [\sum_i n_i c_i^{\gamma+\gamma'}] b_{\gamma'} \\ - \sum_i n_i^2 c_i^\gamma = 0 \end{aligned} \quad (2.13b)$$

$$- \rho(H_q) = 0 \quad (2.13c)$$

If it is assumed that the magnetic field density $\rho(H)$ can be expanded in a complete orthonormal set of

functions $\phi_n(H)$ such that

$$\rho(H) = \sum_n a_n \phi_n(H) \quad (2.14)$$

and

$$\int_0^\infty dH \phi_n(H) \phi_{n'}(H) = \delta_{nn'} \quad (2.15)$$

then the set of equations in Eq (2.13) becomes

$$\begin{aligned} \sum_{n'} \{ \int_0^\infty dH' [\sum_i n_i L(c_i, H) L(c_i, H')] + A g(-\Delta^2) \} \phi_{n'}(H') a_{n'} \\ - \lambda_q \delta(H - H_q) - \sum_\gamma [\sum_i n_i L(c_i, H) c_i^\gamma] b_\gamma \\ - \sum_i n_i^2 L(c_i, H) = 0 \end{aligned} \quad (2.16a)$$

$$\begin{aligned} - \sum_{n'} \int_0^\infty dH' [\sum_i n_i c_i^\gamma L(c_i, H')] \phi_{n'}(H') a_{n'} \\ + \sum_\gamma [\sum_i n_i c_i^{\gamma+\gamma'}] b_{\gamma'} - \sum_i n_i^2 c_i^\gamma = 0 \end{aligned} \quad (2.16b)$$

$$- \sum_{n'} \phi_n(H_q) a_{n'} = 0 \quad (2.16c)$$

Notice that when Eq (2.16a) is multiplied by $\phi_n(H)$ and then integrated over H , the resulting set of equations can be written as

$$\sum_{n'} B_{nn'} a_{n'} - \sum_\gamma D_{n\gamma} b_\gamma - \sum_q C_{nq} \lambda_q = -P_n \quad (2.17a)$$

$$-\sum_n D_{n\gamma} a_n + \sum_{\gamma} E_{\gamma\gamma'} b_{\gamma'} = q_{\gamma} \quad (2.17b)$$

$$-\sum_n C_{nq} a_n = 0 \quad (2.17c)$$

Or, in matrix form, the least-squares minimization problem is

$$\begin{bmatrix} B & -D & -C \\ -\tilde{D} & E & 0 \\ -\tilde{C} & 0 & 0 \end{bmatrix} \begin{bmatrix} a \\ b \\ \lambda \end{bmatrix} = \begin{bmatrix} -p \\ q \\ 0 \end{bmatrix} \quad (2.18)$$

with

$$B_{nn'} = \iint dH dH' \phi_n(H) [\sum_i n_i L(c_i, H) L(c_i, H')] + Ag(-\Delta^2) \phi_n(H') \quad (2.19a)$$

$$C_{nq} = \phi_n(H_q) \quad (2.19b)$$

$$D_{n\gamma} = \int dH \phi_n(H) [\sum_i n_i L(c_i, H) c_i^{\gamma}] \quad (2.19c)$$

$$E_{\gamma\gamma'} = \sum_i n_i c_i^{\gamma+\gamma'} \quad \gamma, \gamma' = 0, 1, 2 \quad (2.19d)$$

$$P_n = \int dH \phi_n(H) [\sum_i n_i^2 L(c_i, H)] \quad (2.19e)$$

$$q_{\gamma} = \sum_i n_i^2 c_i^{\gamma} \quad \gamma = 0, 1, 2 \quad (2.19f)$$

The focus of the problem now lies in finding a solution for the integral $I = \int dH \phi_n(H) L(c, H)$ found in Eqs (2.19a), (2.19c) and (2.19e).

Numerical Solution for the Integral

In order for the integral, I , to be solved analytically, the appropriate forms of the functions $\rho(H)$ and $L(c, H)$ must be known.

Lineshape Function. The lineshape function $L(c, H)$ consists of a contribution from each peak that occurs in a given spectrum such that

$$L(c_i, H) = \sum_{j=1}^m f_j \ell_j(c_i, H) \quad (2.20)$$

where

m = number of peaks in the spectrum

f_j = recoil-free fraction or intensity of the peak

$\ell_j(c, H)$ = function describing the actual shape of individual peaks

In general, the function $\ell_j(c, H)$ is usually assumed to be either a Lorentzian or Gaussian lineshape located at

$$c_j(H) = d_0 + d_1^j H \quad (2.21)$$

where

d_0 is the channel number of the spectrum center

d_1^j is a factor that describes the "shift" of an individual peak with magnetic field

c_j is the resulting channel location of a peak

Therefore, it follows that when $H=0$, each peak will be centered at d_0 . However, the peaks will spread linearly, but differently with varying H .

When a magnetic field causes splitting of the nuclear states, the Mössbauer nucleus, Fe^{57} , has six allowed transitions which will yield a spectrum consisting of six peaks. Assuming a Gaussian lineshape

$$I_j(H) = \frac{e^{-\frac{(Z-h)^2}{2\Gamma^2}}}{\Gamma \sqrt{2\pi}} \quad j = 1 \text{ to } 6 \quad (2.22)$$

with

h = location of the Gaussian peak center

Γ = peak linewidth

By substituting Eq (2.21) for h , Eq (2.22) becomes

$$I_j(c, d_0, d_1^j, \Gamma, H) = \frac{e^{-\frac{(c-d_0-d_1^j H)^2}{2\Gamma^2}}}{\Gamma \sqrt{2\pi}} \quad (2.23)$$

and the integral I is

$$I = \sum_j f_j \int dH \frac{e^{-\frac{(c-d_0-d_1^j H)^2}{2\Gamma^2}}}{\Gamma \sqrt{2\pi}} \phi_n(H) \quad (2.24)$$

Set of Functions ϕ_n . The set of functions ϕ_n must combine to form a distribution of magnetic fields. Based on Eq (2.21), it is clear that a given absorption peak can be moved with varying H . In general, only positive field strength is considered, but by allowing a negative magnetic field H and thereby assuming that $\rho(H)$ is symmetric, an appropriate choice for ϕ_n would be an orthonormal form of the Hermite polynomials.

Starting with the generating function for the Hermite polynomials,

$$e^{-s^2+2sZ} = \sum_0^{\infty} \frac{s^n}{n!} H_n(Z) \quad (2.25)$$

the addition of a weighting factor for orthogonality, $e^{-Z^2/2}$, will yield

$$e^{-Z^2/2} e^{-s^2+2sZ} = \sum_0^{\infty} \frac{s^n}{n!} e^{-Z^2/2} H_n(Z) \quad (2.26)$$

The set of functions are normalized with the constant

$$\frac{1}{\sqrt{2^n n!} \sqrt{\pi}} \text{ such that}$$

$$\frac{e^{-Z^2/2} e^{-s^2/2 + sZ\sqrt{2}}}{4\sqrt{\pi}} = \sum_{n=0}^{\infty} \frac{s^n}{\sqrt{n!}} \frac{e^{-Z^2/2} H_n(Z)}{4\sqrt{\pi} \sqrt{2^n n!}}$$

$$\equiv \sum_{n=0}^{\infty} \frac{s^n}{\sqrt{n!}} h_n(Z) \quad (2.27)$$

where the orthonormal functions $\phi_n(Z)$ are

$$\phi_n(Z) = \frac{e^{-Z^2/2} H_n(Z)}{4\sqrt{\pi} \sqrt{2^n n!}} \quad (2.28a)$$

with the generating function

$$\frac{e^{-Z^2/2} e^{-s^2/2 + sZ\sqrt{2}}}{4\sqrt{\pi}} \quad (2.28b)$$

If the magnetic field density is redefined in terms of a dimensionless variable, Z , then $\rho(Z) = \sum a_n \phi_n(Z)$ with $Z = H/H_0$. Then $\phi_n(H)$ can be replaced with the left hand side of Eq (2.27), and the integral becomes

$$I = \sum_j f_j \int_{-\infty}^{\infty} dH \frac{e^{-\frac{(c-d_0-d_1^j H)^2}{2\Gamma^2}}}{\Gamma\sqrt{2\pi}} \frac{e^{-s^2/2 + sZ\sqrt{2} - Z^2/2}}{4\sqrt{\pi}} \quad (2.29a)$$

which is related to the functions h_n and ℓ_j as

$$I = \sum_j f_j \sum_{n=0}^{\infty} \frac{s^n}{\sqrt{n!}} \int_{-\infty}^{\infty} dH h_n(Z) \ell_j(c, d_0, d_1^j, \Gamma, H) \quad (2.29b)$$

Integral Approximation. In order to find a solution to the integral in Eq (2.29a), the exponential terms must be combined and reduced. First, using the dimensionless variable Z defined earlier, where $H=H_0 Z$, the integral is

$$I = \sum_j f_j \int H_0 dZ \frac{e^{-\frac{(c-d_0-d_1 H_0 Z)^2}{2\Gamma^2}}}{\Gamma \sqrt{2\pi} \frac{4}{\sqrt{\pi}}} \cdot e^{-s^2/2 + sZ\sqrt{2} - Z^2/2} \quad (2.30)$$

Combining the exponential terms yields

$$\begin{aligned} \text{exponent} = & -\frac{Z}{2} \left\{ \frac{d_1^2 H_0^2}{\Gamma^2} + 1 \right\} + Z \left\{ s\sqrt{2} - \frac{d_1 H_0 (c-d_0)}{\Gamma^2} \right\} \\ & - \frac{1}{2} \left\{ s^2 + \frac{(c-d_0)^2}{\Gamma^2} \right\} \end{aligned} \quad (2.31)$$

which further simplifies as

$$\begin{aligned} \text{exponent} = & -\frac{1}{2} \left[\frac{d_1^2 H_0^2 + \Gamma^2}{\Gamma^2} \right] \left\{ \frac{Z^2 - 2Z[\Gamma^2 s\sqrt{2} - d_1 H_0 (c-d_0)]}{\Gamma^2 + (d_1 H_0)^2} \right. \\ & \left. + \frac{[\Gamma^2 s^2 + (c-d_0)^2]}{\Gamma^2 + (d_1 H_0)^2} \right\} \end{aligned} \quad (2.32)$$

Finally, by completing the square the exponent is

$$\begin{aligned}
& - \frac{1}{2} \left[\frac{d_1^2 H_o^2 + \Gamma^2}{\Gamma^2} \right] \left\{ Z - \left[\frac{\Gamma^2 s \sqrt{2} - d_1 H_o (c - d_o)}{\Gamma^2 + (d_1 H_o)^2} \right]^2 \right. \\
& \left. + \frac{\Gamma^2 s^2 + (c - d_o)^2}{\Gamma^2 + (d_1 H_o)^2} - \left(\frac{\Gamma^2 s \sqrt{2} - d_1 H_o (c - d_o)}{\Gamma^2 + (d_1 H_o)^2} \right)^2 \right\} \quad (2.33)
\end{aligned}$$

Since the last two terms of the exponent are independent of Z , integration of the exponential yields an I such that

$$\begin{aligned}
I = \sum_j f_j \frac{H_o \exp}{4\sqrt{\pi} \sqrt{\Gamma^2 + (d_1 H_o)^2}} \left\{ -\frac{1}{2} \left[s^2 + \frac{(c - d_o)^2}{\Gamma^2} \right. \right. \\
\left. \left. - \frac{(\Gamma^2 s \sqrt{2} - d_1 H_o (c - d_o))^2}{\Gamma^2 (\Gamma^2 + (d_1 H_o)^2)} \right] \right\} \quad (2.34)
\end{aligned}$$

Where both d_1 and Γ may be subscripted j to correspond with each peak. Assuming that the linewidth does not vary, Eq (2.34) can be rewritten as

$$I = \sum_j f_j \frac{H_o}{4\sqrt{\pi} \sqrt{\Gamma^2 + (d_1^j H_o)^2}} \exp \left\{ -\frac{1}{2} (a^2 s^2 + b s + c) \right\} \quad (2.35)$$

with

$$a^2 = 1 - \frac{2\Gamma^2}{\Gamma^2 + (d_1^j H_o)^2} = \frac{(d_1^j H_o)^2 - \Gamma^2}{(d_1^j H_o)^2 + \Gamma^2} \quad (2.36a)$$

$$b = \frac{2\sqrt{2} d_1^j H_0 (c-d_0)}{\Gamma^2 + (d_1^j H_0)^2} \quad (2.36b)$$

$$c' = \frac{(c-d_0)^2}{\Gamma^2} - \frac{(d_1^j H_0)^2 (c-d_0)^2}{\Gamma^2 (\Gamma^2 + (d_1^j H_0)^2)} = \frac{(c-d_0)^2}{\Gamma^2 + (d_1^j H_0)^2} \quad (2.36c)$$

Therefore, the exponential term in c' can be placed with the constant to give

$$I = \sum_j f_j \frac{H_0 e^{-\frac{(c-d_0)^2}{2(\Gamma^2 + (d_1^j H_0)^2)}}}{\frac{4\sqrt{\pi}}{\sqrt{\Gamma^2 + (d_1^j H_0)^2}}} \exp(-\frac{1}{2} [a^2 s^2 + bs]) \quad (2.37)$$

This expression is then defined as

$$I \equiv \sum_j f_j \sum_n \frac{s^n}{\sqrt{n!}} J_n(c, d_0, d_1^j, \Gamma, H_0) \quad (2.38a)$$

which is equivalent to the relation

$$\sum_j f_j \sum_n \frac{s^n}{\sqrt{n!}} \int_{-\infty}^{\infty} dH h_n\left(\frac{H}{H_0}\right) \ell_j(c, d_0, d_1^j, \Gamma, H) \quad (2.38b)$$

so that the number of functions J used to approximate the integral is directly related to the number of Hermite polynomials in the description of $\rho(H)$.

If the exponent in Eq (2.37) is expanded in a series where

$$e^{-\frac{1}{2}(a^2 s^2 + bs)} = 1 - \frac{1}{2}(a^2 s^2 + bs) + \frac{1}{8}(a^2 s^2 + bs)^2 - \frac{1}{48}(a^2 s^2 + bs)^3 + \dots \quad (2.39)$$

or

$$e^{-\frac{1}{2}(a^2 s^2 + bs)} = 1 + s\left(\frac{-b}{2}\right) + \frac{s^2}{\sqrt{2!}}\left(\frac{-a^2}{2} + \frac{b^2}{8}\right)\sqrt{s!} + \frac{s^3}{\sqrt{3!}}\left(\frac{a^2 b}{4} - \frac{b^3}{48}\right)\sqrt{3!} + \dots \quad (2.40)$$

then it follows that

$$J_0 = \frac{H_0 e^{-\frac{1}{2} \frac{(c-d_0)^2}{\Gamma^2 + (d_1^j H_0)^2}}}{\sqrt[4]{\pi} \sqrt{\Gamma^2 + (d_1^j H_0)^2}} \quad (2.41a)$$

$$J_1 = \frac{H_0 e^{-\frac{1}{2} \frac{(c-d_0)^2}{\Gamma^2 + (d_1^j H_0)^2}}}{\sqrt[4]{\pi} \sqrt{\Gamma^2 + (d_1^j H_0)^2}} \left(\frac{-b}{2}\right) \quad (2.41b)$$

$$J_2 = \frac{H_0 e^{-\frac{1}{2} \frac{(c-d_0)^2}{\Gamma^2 + (d_1^j H_0)^2}}}{\sqrt[4]{\pi} \sqrt{\Gamma^2 + (d_1^j H_0)^2}} \left(\frac{-a^2}{2} + \frac{b^2}{8}\right)\sqrt{2} \quad (2.41c)$$

Recursion Relation

In order for the functions J_n to be generated in a computer solution, it would be advantageous to find these functions by recursion. Since the Hermite functions satisfy the recursion relation

$$2X H_n(X) = H_{n+1}(X) + 2n H_{n-1}(X) \quad (2.42)$$

and recalling that the Hermites are generated by the relation

$$e^{-s^2/2 + 2sX} = \sum_0^{\infty} \frac{s^n}{n!} H_n(X) \quad (2.26)$$

it is evident that the functions J_n can be found by recursion

$$e^{-\frac{1}{2}(a^2 s^2 + bs)} = e^{-s^2/2 + 2sX} \quad (2.43)$$

Solving for the term X in Eq (2.43) yields

$$X = \frac{-b}{2\sqrt{2}a} = \frac{d_1^j H_0(d_0 - c)}{\sqrt{(d_1^j H_0)^4 - \Gamma^4}} \quad (2.44)$$

with a and b as defined in Eq (2.36). As a result, from Eq (2.26) it follows that

$$e^{-\frac{1}{2}(a^2 s^2 + bs)} = e^{-s^2/2 + 2sX} = \sum_0^{\infty} \frac{s^n}{n!} \left(\frac{a}{\sqrt{2}}\right)^n H_n(X) \quad (2.45)$$

Furthermore, if

$$N(c, d_1^j, H_0, d_0, \Gamma) \equiv \frac{H_0 e^{-\frac{1}{2} \frac{(c-d_0)^2}{\Gamma^2 + (d_1^j H_0)^2}}}{4\sqrt{\pi} \sqrt{\Gamma^2 + (d_1^j H_0)^2}} \quad (2.46)$$

it is evident that

$$\begin{aligned} N e^{-\frac{1}{2}(a^2 s^2 + bs)} &= \sum \frac{s^n}{\sqrt{n!}} J_n(c, d_1^j, H_0, d_0, \Gamma) \\ &= N \sum \frac{s^n}{n!} \left(\frac{a}{\sqrt{2}}\right)^n H_n\left(\frac{-b}{2\sqrt{2}a}\right) \end{aligned} \quad (2.47)$$

and therefore each of the functions J_n can be found where

$$J_n(c, d_1^j, H_0, d_0, \Gamma) = \frac{N}{\sqrt{n!}} \left(\frac{a}{\sqrt{2}}\right)^n H_n\left(\frac{-b}{2\sqrt{2}a}\right) \quad (2.48)$$

And finally, these functions are related to the original integral as

$$\int dH \phi_n(H) L(c, H) = \sum_j f_j J_n(c, d_1^j, H_0, d_0, \Gamma)$$

In order to find the functions J_n without evaluating each of the Hermites directly, let $h_n(X) = a^n H_n(X)$ so that Eq (2.42) becomes

$$\frac{2Xh_n(X)}{a^n} = \frac{h_{n+1}(X)}{a^{n+1}} + \frac{2n h_{n-1}(X)}{a^{n-1}} \quad (2.49a)$$

or

$$2(Xa)h_n(X) = h_{n+1}(X) + 2(na^2)h_{n-1}(X) \quad (2.49b)$$

Now if $j_n = h_n / \sqrt{n!}$, then $h_n = j_n \sqrt{n!}$ and Eq (2.49b) is

$$2(Xa)j_n \sqrt{n!} = j_{n+1} \sqrt{(n+1)!} + 2(na^2)j_{n-1} \sqrt{(n-1)!} \quad (2.50)$$

which reduces to

$$j_{n+1} = \frac{2a}{\sqrt{n+1}} [Xj_n - a\sqrt{n} j_{n-1}] \quad (2.51)$$

Since the functions J_n are related to j_n as

$$J_n(c, d_1^j, H_0, d_0, r) = \frac{N}{(\sqrt{2})^n} j_n \quad (2.52)$$

j_n can be redefined as $j_n' = Nj_n$ and with $H_0 = 1$ and $H_1 = 2X$, then $j_0' = N$ and $j_1' = 2aXN$, so that the full function can be generated from Eq (2.51). Returning to the integral, it is evident that

$$\int dH \phi_n(H) L(c, H) = \sum_j f_j \frac{j_n'}{(\sqrt{2})^n} \quad (2.53)$$

which is defined as $r_n(c)$.

$$r_n(c) \equiv \frac{1}{(\sqrt{2})^n} \sum_j f_j j_n' = \int dH \phi_n(H) L(c, H) \quad (2.54)$$

Replacing the integrals in the matrix coefficients of

Eq (2.20) gives

$$B_{nn'} = \sum_i n_i r_n(c_i) r_{n'}(c_i) + \int dH \phi_n(H) Ag(-\Delta^2) \phi_{n'}(H) \quad (2.55a)$$

$$C_{nq} = \phi_n(H_q) \quad (2.55b)$$

$$D_{n\gamma} = \sum_i n_i r_n(c_i) c_i^\gamma \quad (2.55c)$$

$$E_{\gamma\gamma'} = \sum_i n_i c_i^{\gamma+\gamma'} \quad (2.55d)$$

$$P_n = \sum_i n_i^2 r_n(c_i) \quad (2.55e)$$

$$q_\gamma = \sum_i n_i^2 c_i^\gamma \quad (2.55f)$$

It is evident that with $r_n(c)$ known, all of the matrix coefficients can be determined with the exception of $B_{nn'}$ and C_{nq} . The smoothing function

$$\int dH \phi_n(H) Ag(-\Delta^2) \phi_{n'}(H') \quad (2.56)$$

must be computed. When the functions ϕ_n are assumed to be Hermite polynomials, the operator $g(-\Delta^2)$ must be chosen to provide a measure of roughness that relates to the form of these functions. Since the Hermite polynomials are Harmonic oscillator functions, the measure of roughness can be appropriately defined by the operator $g(\frac{1}{2}(Z^2 - \frac{d^2}{dZ^2}))$ as

$$R_o = \int dH \phi_n(H) g\left(\frac{1}{2}\left(Z^2 - \frac{d^2}{dZ^2}\right)\right) \phi_n(H') \quad (2.57)$$

The use of this factor in the solution of the Harmonic oscillator is well known, where

$$\frac{1}{2}\left(Z^2 - \frac{d^2}{dZ^2}\right)h_n(Z) = \left(n + \frac{1}{2}\right)h_n(Z) \quad (2.58)$$

Therefore, the roughness term is

$$R_o = A \int dH dH' \phi_n(H) g\left(\frac{1}{2}\left(Z^2 - \frac{d^2}{dZ^2}\right)\right) \phi_n(H') \quad (2.59)$$

which, upon integration, is

$$R_o = A H_o \delta_{nn'} g\left(n + \frac{1}{2}\right) = A H_o \delta_{nn'} \sum_{r=1}^R a_r \left(n + \frac{1}{2}\right)^r \quad (2.60)$$

By defining the operator as shown, the solution of the smoothing function is reduced to an arbitrary series in $\left(n + \frac{1}{2}\right)$ consisting of R terms. The sum of this series is added to the diagonal coefficients of $B_{nn'}$. The quantities C_{nq} are found in a more straightforward manner since these coefficients are simply the Hermite functions evaluated for the arguments H_q (really H_q/H_o).

Once all of the matrix coefficients are known, the matrix problem can be solved for the "optimum" values of a_n , b_γ , and λ_q . Using these values, the fit of the magnetic

field density can be found by the expression $\rho(H) = a_n \phi_n(H)$
and the fit spectrum is determined from a modification of
Eq (2.2).

III. Computer Program Development

Two separate programs were written according to the theory discussed in Chapter II. These programs have been designated RPARAM and MOSFIT. The sole purpose of RPARAM is to calculate and store the data independent integral values called $r_n(c)$ in Chapter II. Program MOSFIT solves the minimization problem, then calculates and plots the magnetic field density $\rho(H)$. Once the $\rho(H)$ is appropriately modelled, the fit spectrum is computed and plotted. It is evident that this programming can be divided into three steps:

1. Computation of $r_n(c)$
2. Determination of $\rho(H)$
3. Computation of Fit Spectrum

This chapter will discuss the computer program development as outlined by the three categories above. A full listing of the programming may be found in Appendix B.

Computation of $r_n(c)$

Since the computation of the parameters $r_n(c)$ is independent of the actual counting data, a separate program was devised to calculate and store the values of $r_n(c)$ for a given Mössbauer nucleus. The flowchart for this program is shown in Figure 3. Program RPARAM is clearly divided into four subroutines, FIX, CONS, INTEG, and RITEO.

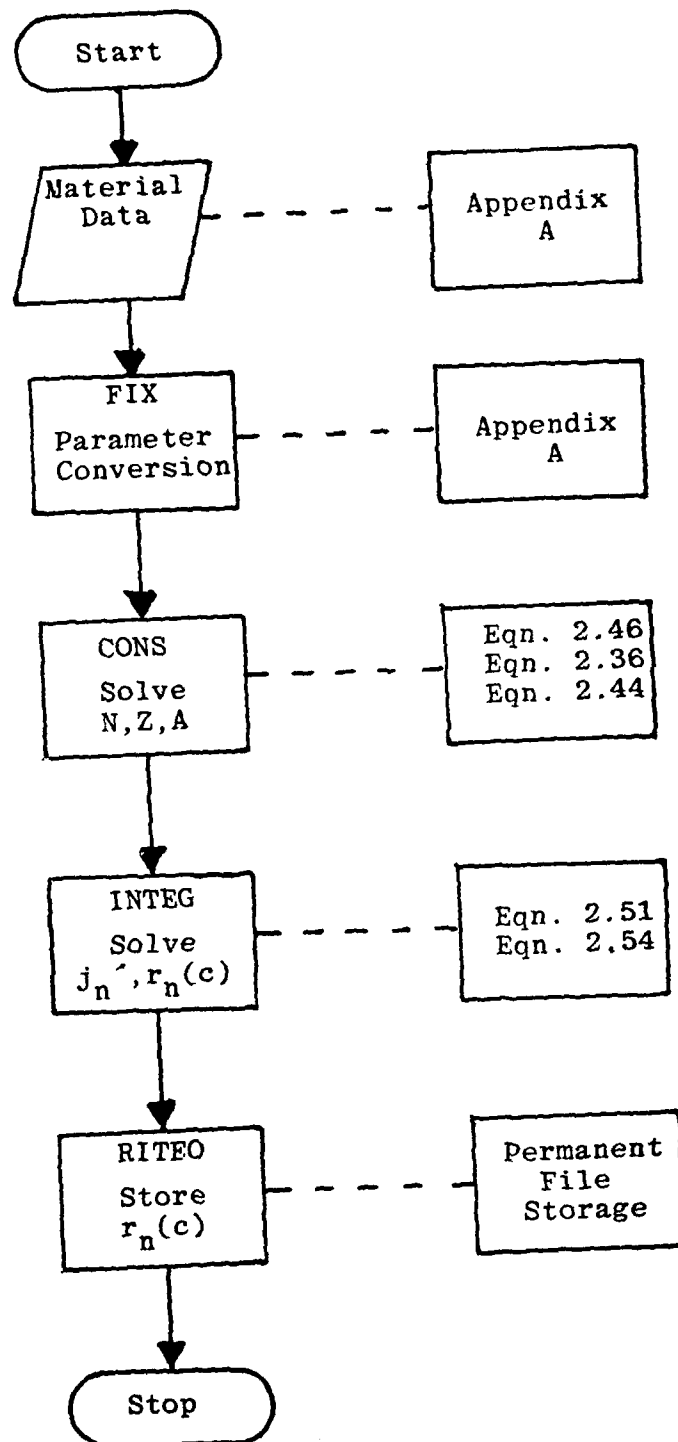


Figure 3. Flow Diagram for RPARAM

Subroutine FIX. The program RPARAM requires the input of the values d_1 , Γ , f_j , H_0 , d_0 for the Mössbauer nucleus studied. These values are material dependent and can be determined by examination of the spectroscopic characteristics of the nucleus in question. The values for Fe^{57} have been computed in Appendix A and are shown in Table I.

TABLE I
Input Parameters for Fe^{57}

j	$d_1(\text{nm})$	f	$\Gamma(\text{mm/s})$	$d_0(\text{mm/s})$	$H_0(\text{kOe})$
1	-.2437	3	.23	.258	400
2	-.1413	2	.23	*	*
3	-.0393	1	.23	*	*
4	.0393	1	.23	*	*
5	.1413	2	.23	*	*
6	.2437	3	.23	*	*

* d_0 and H_0 are independent of j

It is clear that this data is found in a variety of units. The units shown in Table I are those generally found in the literature for each parameter. For this data to be useful in relation to the theory developed in Chapter II, all of the parameters must be found in terms of channel number. The purpose of subroutine FIX is to convert the input data to

channel data. The values of d_1 , d_0 , and Γ can be converted to channel data with two conversion factors. Since two of the parameters are already in units of millimeters/second, it is advantageous to first convert d_1 from nuclear magnetons to mm/s. This can be accomplished using the conversion factor shown

$$\text{CONV} = 3.1574417 \text{ E-12 KeV/nm-kOe} \quad (3.1)$$

in combination with the energy of the nuclear transition and the speed of light. Therefore,

$$d_1(\text{mm/s-kOe}) = d_1(\text{nm}) \cdot \text{CONV} \cdot c(\text{mm/s}) / E_0(\text{KeV}) \quad (3.2)$$

so that $d_1\text{H}_0$ will be in units of mm/s. Finally, each of the parameters is changed to channel data by a factor that relates velocity to channel number. This factor results from a least-squares fit of channel number to velocity developed by Captain B. E. Pate (Ref 13). Captain Pate found a given velocity to be related to channel number as

$$\text{channel} = (\text{velocity} + 9.795990) / .04819964$$

where

$$\text{one channel} = .04819964 \text{ mm/s}$$

These relations are incorporated into subroutine FIX to convert from velocity to channel data.

Subroutine CONS. A determination of the parameters $r_n(c)$ first requires the computation of several terms that are used in this calculation. This subroutine solves for

these terms as outlined by the flowchart included in Appendix B.

The first set of values calculated are the a terms found in the recursion relation (Eq (2.51)) and defined in Eq (2.36a). Since these a terms vary with d_1^j , six values are computed to correspond to the six absorption peaks in the spectrum. The evaluation of a is found in line 23 of RPARAM as

$$A(J) = \text{SQRT}(((D1(J)*HO)**2 - GMMA(J)**2)/((D1(J)*HO)**2 + GMMA(J)**2)) \quad (3.3)$$

The other terms to be evaluated are the argument, X , of the j_n function in the recursion relation as well as the constant N . The argument X is defined in Eq (2.44)

$$X = \frac{d_1^j H_o (d_o - c)}{\sqrt{(d_1^j H_o)^4 - r^4}}$$

and the value of N can be found by Eq (2.46), where

$$N = \frac{H_o e^{-\frac{1}{2} \frac{(c-d_o)^2}{r^2 + (d_1^j H_o)^2}}}{\sqrt[4]{\pi} \sqrt{r^2 + (d_1^j H_o)^2}}$$

It is evident that each of these terms vary with both the channel number and the absorption peak in question. The X

is found in line 27 of RPARAM by

$$Z(J,CI) = D1(J)*HO*(DO-CI)/SQRT((D1(J)*HO)**4 - GMMA(J)**4) \quad (3.4)$$

The constant N is computed in two parts. NX represents the exponential part of N while NC combines the terms not associated with the exponent. As a result, N is found in three steps:

$$NX = EXP(-(CI-DO)**2/(2.*(GMMA(J)**2 + (D1(J)*HO)**2))) \quad (3.5a)$$

$$NC = HO/(PI**(1./4.)*SQRT(GMMA(J)**2 + D1(J)**2*HO**2)) \quad (3.5b)$$

$$N(J,CI) = NC*NX \quad (3.5c)$$

Each value of A, Z, and N are used in turn to compute the functions j_n and the $r_n(c)$ parameters in subroutine INTEG.

Subroutine INTEG. This subroutine finds the functions j_n by means of the recursion relation presented in Eq (2.51), where j_0 and j_1 are known. Each of these functions will vary with channel number and absorption peak. The recursion relation is found in line 47 of RPARAM and is coded as

$$FNJ(J,S+1,CI) = (2.*A(J)/SQRT(S+1))*(J,CI)*FNJ(J,S,CI) - A(J)*FNJ(J,S-1,CI)*SQRT(S1)) \quad (3.6)$$

The values of $r_n(c)$ are subsequently determined in line 50 where

$$R(S,CI) = F(J)*(1./((SQRT(2.))*S)*FNJ(J,S,CI) + R(S,CI) \quad (3.7)$$

which corresponds to Eq (2.54). A flowchart of this routine can be found in Appendix B.

Subroutine RITEO. The function of RITEO is simply to write the values of $r_n(c)$ for permanent files storage. It is designed to write a maximum of five values per line in an E14.7 format.

Determination of $\rho(H)$

The magnetic field density is determined in MOSFIT using values found in the least-squares minimization. The subroutines of interest in this case are READN, COEFF, MATR1, HERMIT, MESCHP, MAGFD and PLTMAG. A generalized flowchart of the entire MOSFIT program is found in Figures 4 and 5.

Subroutine READN. Subroutine READN is designed to read the experimental data and the previously computed values of $r_n(c)$ from a data tape. The data is read from TAPE9 in an I3,10F7.0 format. This format corresponds to the data as recorded by the multichannel analyzer. The $r_n(c)$ values are read from TAPE8 in format chosen to correspond with RITEO.

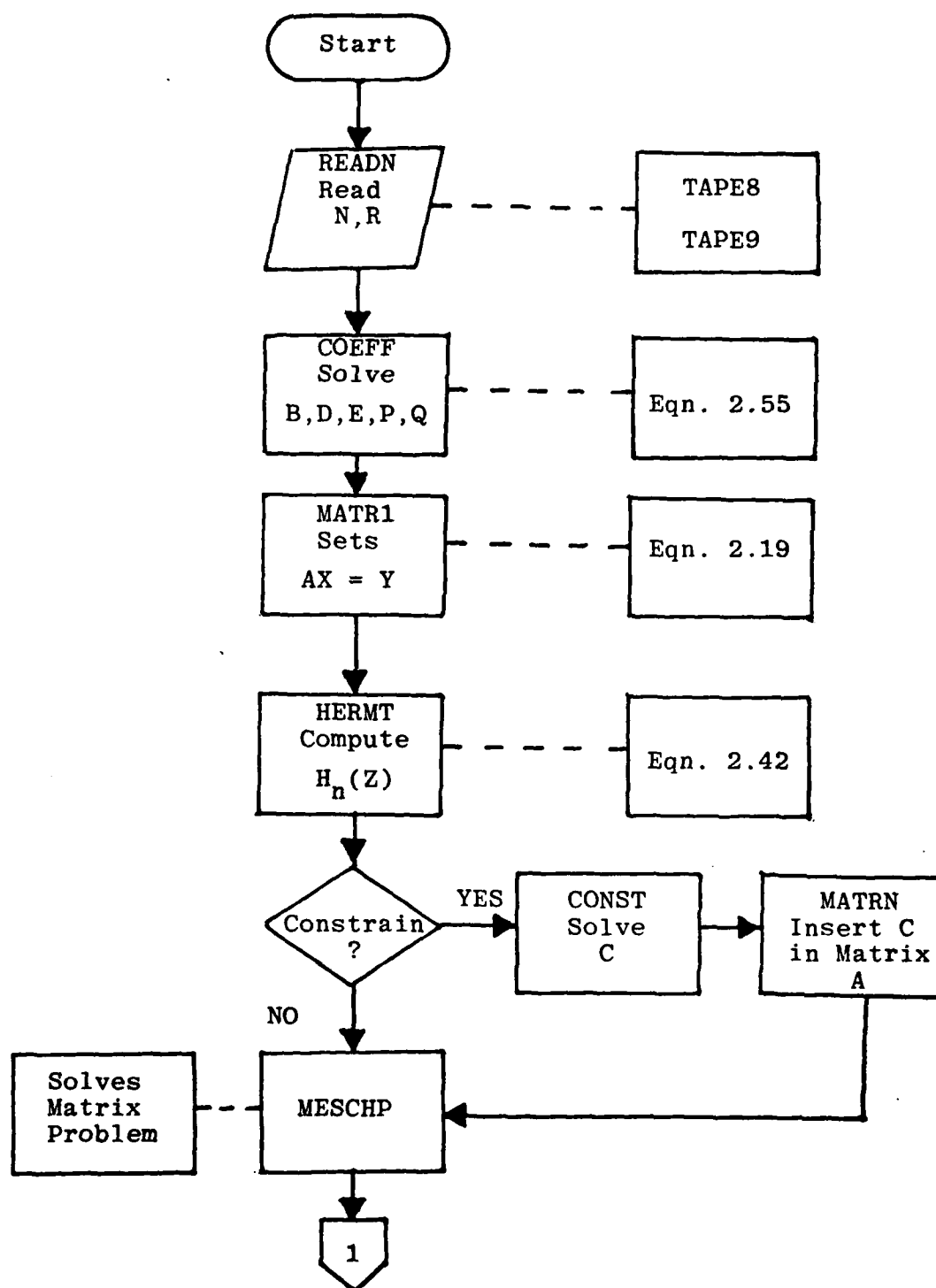


Figure 4. Generalized Flowchart for MOSFIT pt. I

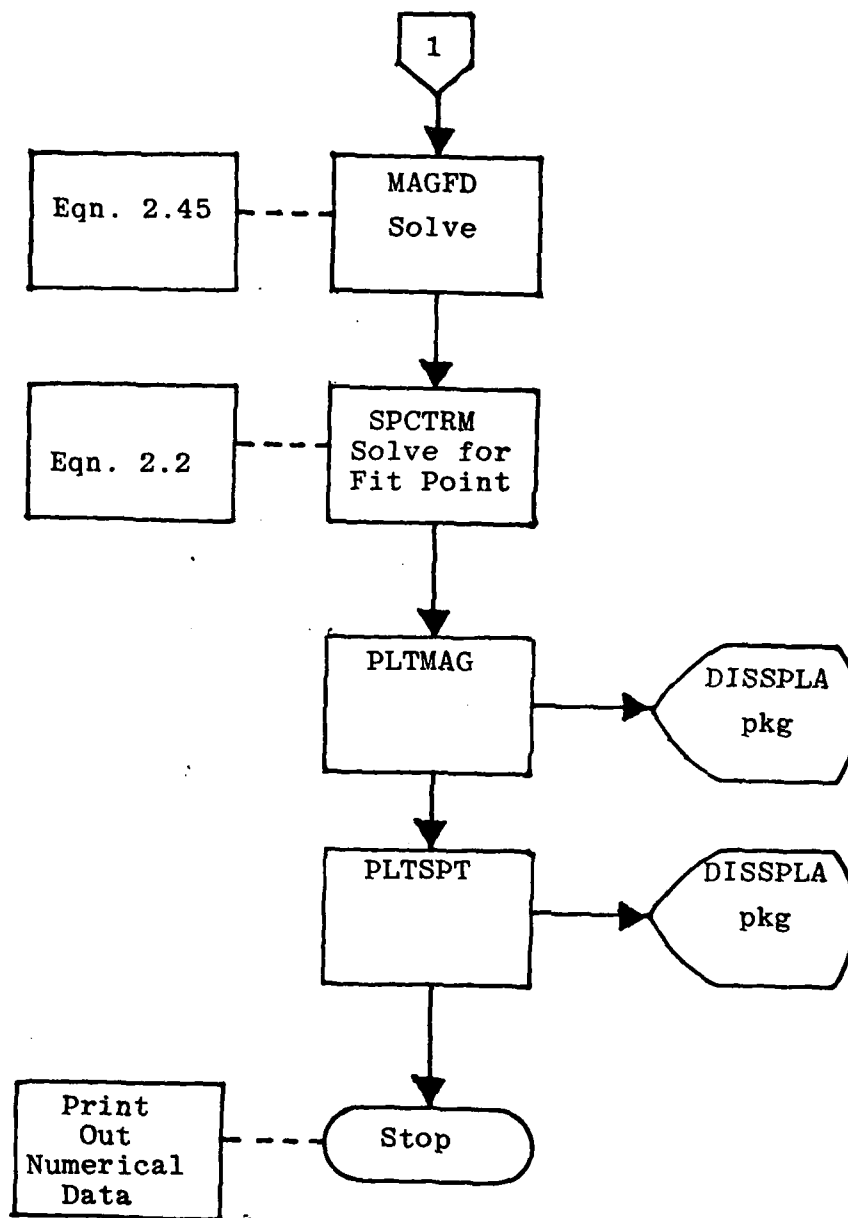


Figure 5. MOSFIT Flowchart pt. II

Subroutine MATR1. The utility of this routine is to assign the previously computed coefficients to a matrix A so the matrix problem $AX = Y$ can be solved. This routine could be incorporated into the subroutine COEFF if desired.

Subroutine HERMIT. Subroutine HERMIT calculates and stores the $n+1$ Hermite polynomials used in the computation of $\rho(H)$. The range of magnetic field strength is divided into 100 sub-divisions and the set of polynomials is evaluated for each increment of H/H_0 . The polynomials are generated using the known values of H_0 and H_1 and the Hermite recursion relation in Eq (2.42)

$$2XH_n(X) = H_{n+1}(X) + 2nH_{n-1}(X)$$

This relation is coded in line 174 of MOSFIT as

$$\begin{aligned} HP(I, S+1) = & 2. * (H(I) / HO) * HP(I, S) \\ & - 2. * S * HP(I, S-1) \end{aligned} \quad (3.10)$$

where the index I represents the increment of the field strength and S represents the polynomial number from 0 to n.

Subroutine MESCHP. Subroutine MESCHP solves the matrix problem by performing a Choleski decomposition on matrix A. (Ref 14). The program was written by Dr. Shankland and is found in a library cataloged as BINDEK, CY=1, ID=T760142 in the AFIT system. The arguments for the subroutine are:

A - the coefficient matrix of the problem
 NA - the dimensioned size of matrix A
 K - the actual size of A ($K \leq NA$)
 Y - the solution of matrix A
 1 - indicates Y is a vector dimensioned (NAx1)
 IE - error indicator (no input needed)
 D - scratch vector must be dimensioned to at least length K

The answers to the matrix problem are found in Y at the completion of the computation.

Subroutine MAGFD. This routine uses the solution vector and the Hermite polynomials HP(I,S) to model the magnetic field density. Since

$$\rho(Z) = \sum_n a_n H_n(Z)$$

and the expansion coefficients a_n are found in the solution vector Y, it follows that

$$RHO(I) = Y(S)*HP(I,S) + RHO(I) \quad (3.11)$$

when the equation is summed over S. Equation (3.11) is found in line 197 of MOSFIT with the addition of constants for orthogonality and normality. This equation is used to find the value of $\rho(Z)$ at the incremented value of Z.

Subroutine PLTMAG. Simply put, PLTMAG uses library software (the DISSPLA package) to plot the values of RHO(I) versus the incremented values of the magnetic field strength H(I). It requires DISSPLA, ID=LIBRARY, SN=ASD be attached as a library.

The solution of the magnetic field density can be more clearly understood by examining the flowcharts for COEFF, HERMIT, and MAGFD that are contained in Appendix B.

Computation of Fit Spectrum

With the bulk of the calculations done, the final step is to compute the fit spectrum. The fit spectrum is found using the RHO(I) previously computed and the single subroutine SPCTRM.

Subroutine SPCTRM. The fit spectrum can be found in two ways. Once the minimized parameters a_n , b_γ and λ_q have been found in the solution vector Y, these values can be applied in Eq (2.2) to find the fit spectrum. The integral is approximated by the rectangular method:

$$\Delta H \sum_{\alpha} \rho(H^{\alpha}) L(c, H^{\alpha})$$

using the $\rho(H)$ calculated in MAGFD and the lineshape formula found in Eq (2.24). The results is coded in MOSFIT as

$$RL(I) = F(K)*EXP(EX)/(GMMA(J)*SQRT(2.*PI))*DELH*RHO(J) + RL(I) \quad (3.12)$$

where each of the parameters Γ , d_1 , and d_0 are corrected by subroutine FIX as in RPARAM. An alternate method for determining the spectrum has also been programmed where the integral values $r_n(c)$ and the computed coefficients a_n are used. Since

$$\int \phi_n(H) L(c, H) dH \equiv r_n(c)$$

the integral part of Eq (2.2) can be found as

$$\sum_n a_n r_n(c)$$

so that the parameters Γ , d_1 , d_0 , and subroutine FIX are not necessary. This method has two advantages:

1. Computation time is greatly reduced.
2. The analytical solution in $r_n(c)$ is expected to be more accurate than the corresponding numerical integration.

An outline of the fitting method using the $r_n(c)$ values is flowcharted in Appendix B.

Subroutine PLTSPT. This routine also uses the DISSPLA package to plot the fit spectrum. The fit points $RL(I)$ are plotted versus the channel number C . For comparative purposes, the actual data $N(C)$ is printed on the same plot.

Other Routines

In addition to the programming previously discussed, there are two essential subroutines that have not been written but are necessary for the solution of this problem.

Subroutine CONST. This subroutine is necessary for the application of constraints in the problem. The principle purpose of CONST would be to calculate the matrix coefficients

C found in Eq (2.55). The computed points $\text{RHO}(I)$ are analyzed for negative values and the index I of the points to be constrained are noted. Using the Hermite values already computed, the coefficients C are simply the n Hermite values of each negative point I_{α} .

Subroutine MATRN. MATRN would be analogous to subroutine MATR1; however, it would only assign the coefficients C to the matrix A . Matrix is dimensioned to allow the addition of constraints as necessary.

Besides subroutines CONST and MATRN, an additional routine, SMOOTH, has been written. SMOOTH functions as a test of accuracy in the fitting procedure. This routine calculates the value of the system S (Eq (2.12)) after the least-squares minimization. This value is used to determine when a sufficient number of Hermit polynomials has been used to describe $\rho(H)$. This procedure is detailed in Chapter V.

IV. Program Validation

In order for a computer program to effectively solve a desired problem, the program must be examined to determine whether it is functionally and computationally accurate. An excellent discussion on the framework and procedures of program testing can be found in the literature (Ref 15).

The individual subroutines of both programs were examined to determine the correctness and accuracy of the numerical calculations. In addition, the function of non-computational routines was investigated to assure desired performance. The current programming is a result of corrections made through this somewhat iterative testing procedure. Therefore, corrected errors will not be discussed. However, validation procedures and numerical testing of these programs are included.

Program RPARAM was initially examined with regard to the input data (as described in Appendix A) and the lineshape function. It was important for the data and the lineshape function (Eq (2.21)) to produce a curve comparable to an Fe^{57} spectrum. This test also helps support the correction factors used in subroutine FIX. The result of this examination of data and lineshape can be seen in Figure 6. This plot was generated using the data in Table I (as corrected by subroutine FIX). The general lineshape correlates with the expected results.

LINESHAPE AND DATA TEST

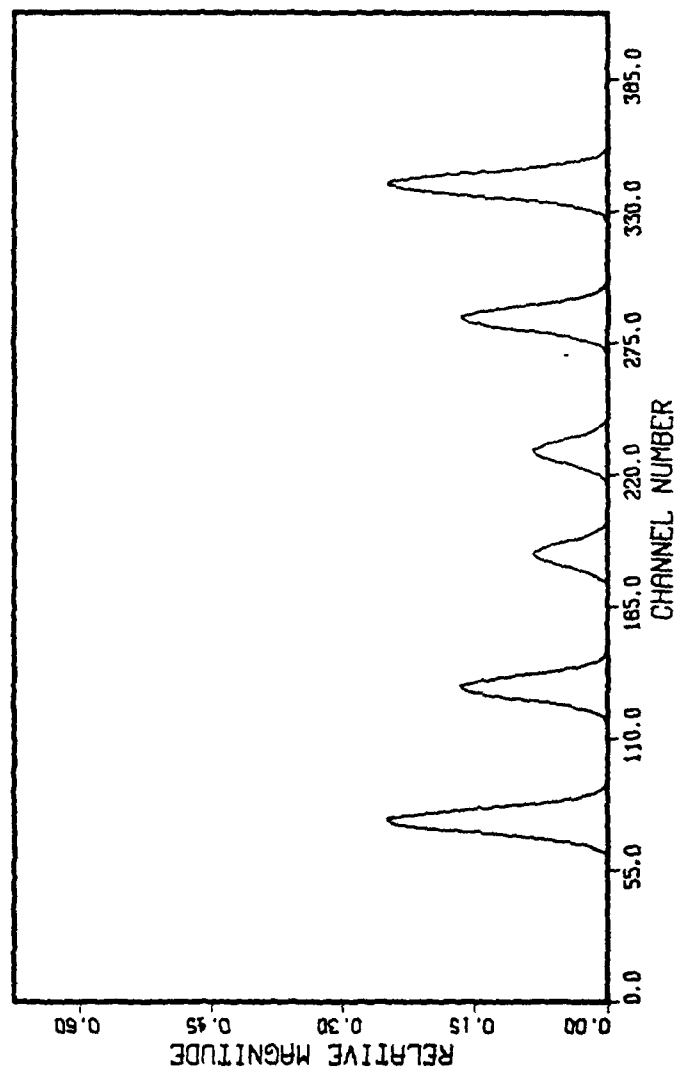


Figure 6. Examination of the General Lineshape Produced with Given Data

Next, the computational accuracy of RPARAM was examined. It was arbitrarily decided to examine the values of all parameters evaluated at $J=1$, $CI=200$ and $S=1$ to 4. The relations FNJ (corresponding to j_n) were hand calculated by the following two equations:

$$FNJ_S = \frac{A(J)^S H_S(Z)}{\sqrt{S!}} \quad (a)$$

$$FNJ_{S+1} = \frac{2A(J)}{\sqrt{S+1}} [Z(FNJ_S) - A\sqrt{S} (FNJ_{S-1})] \quad (b)$$

and computationally determined by the programmed recursion method as well as from the actual series (analytic) solution (Eq (2.40)). The results were vaforable as shown in Table II.

TABLE II
Evaluation of FNJ

S	FNJ (a)	FNJ (b)	Computer Recursion
1	-.1298061	-.1298061	-0.1298062505182
2	-1.3986532	-1.3986533	-1.39865339369
3	.3162459	.3162459	0.3162465049902
4	2.395768	2.3957681	2.3957683649

In addition, $A(1)$ was found to correspond to the calculated value of .9987102 while Z varied slightly in the third decimal place.

The final subroutine RITEO was assumed to be functionally correct based on examination of the data tape generated.

Program MOSFIT was also examined for proper performance. Subroutine READN was tested simply by writing out the data read into the program and comparing the printed results with the actual data files. Subroutine COEFF was tested with simple integer values for $r_n(c)$ and 10 channels. Each matrix coefficient was calculated by hand and compared to the results from COEFF using the same data. The computed values were found to be in agreement with those that were hand calculated. The routine MATR1 was tested by printing out the values of A and Y in the matrix problem $AX = Y$. The matrix A was symmetric as expected and the coefficients corresponded correctly with those computed in COEFF. HERMIT was found to correctly compute the Hermite polynomials $H_n(H/H_0)$ based on a comparison between the computed Hermites and those hand calculated from the known polynomial forms, i.e.,

$$H_0(Z) = 1$$

$$H_1(Z) = 2Z$$

$$H_2(Z) = 4Z^2 - 2$$

$$H_3(Z) = 8Z^3 - 12Z$$

etc.

One of the fundamental subroutines is MESCHP which solves the matrix problem using a Choleski decomposition of

matrix A. This routine was tested on a simple 2x2 matrix problem to ascertain its computational accuracy. Using the problem

$$\begin{bmatrix} 2 & 1 \\ 1 & 1 \end{bmatrix} \begin{bmatrix} x \\ y \end{bmatrix} = \begin{bmatrix} 4 \\ 3 \end{bmatrix}$$

the routine solved x as 1 and y as 2, which is correct.

The subroutine MAGFD was analyzed by using a single Hermite to model the magnetic field density so that the plotted $\rho(H)$ should correspond to the known shape of the Hermite used. Using H_0 and the orthogonality factor $e^{-z^2/2}$, the subroutine generated a Gaussian centered at 0, corresponding to a plot of the Hermite. Neither plot routine was tested independently, but in the course of other test procedures, the plotting functioned successfully.

Finally, the functional accuracy of the entire program was tested using data with a known $\rho(H)$. This data was generated using a magnetic field density of

$$\rho(Z) = \Sigma e^{-Z^2/2} (H_0(Z) + \frac{1}{6} H_2(Z))$$

and a linear background of 100 counts per channel. The resulting spectrum and magnetic field density can be seen in Figures 7 and 8, respectively. The test procedure used this generated counting data and the previously computed $r_n(c)$ values in program MOSFIT. It is evident that if the program is operating properly, the plots resulting from the

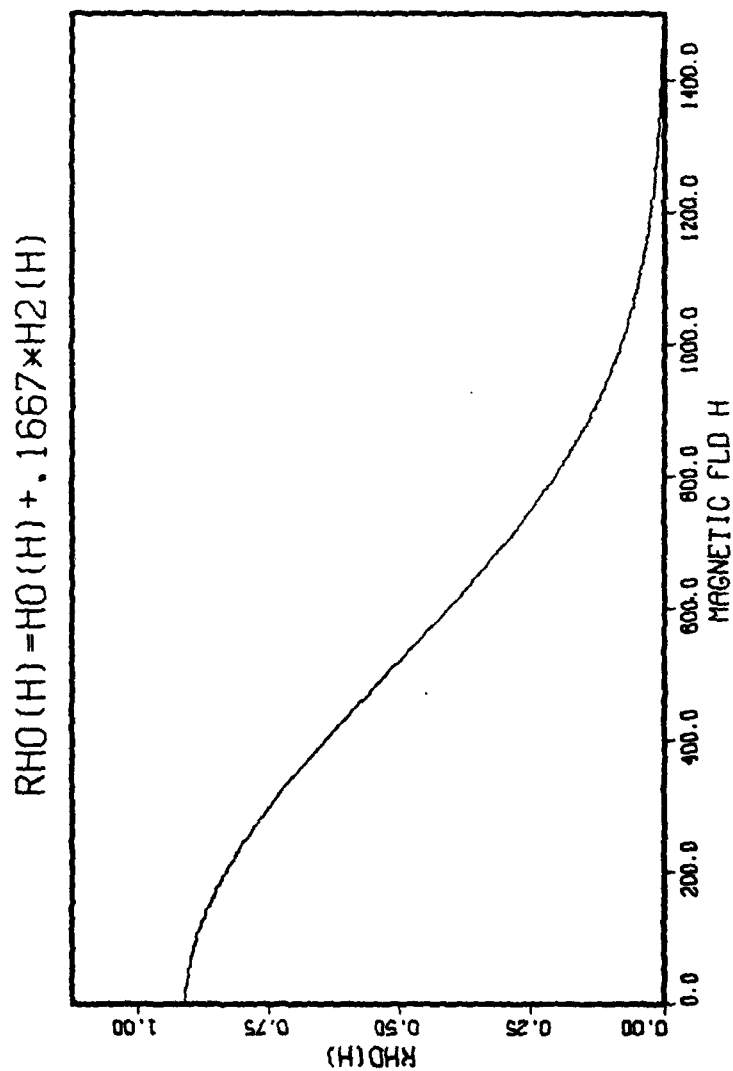


Figure 7. Magnetic Field Density Used to Generate Test Spectrum

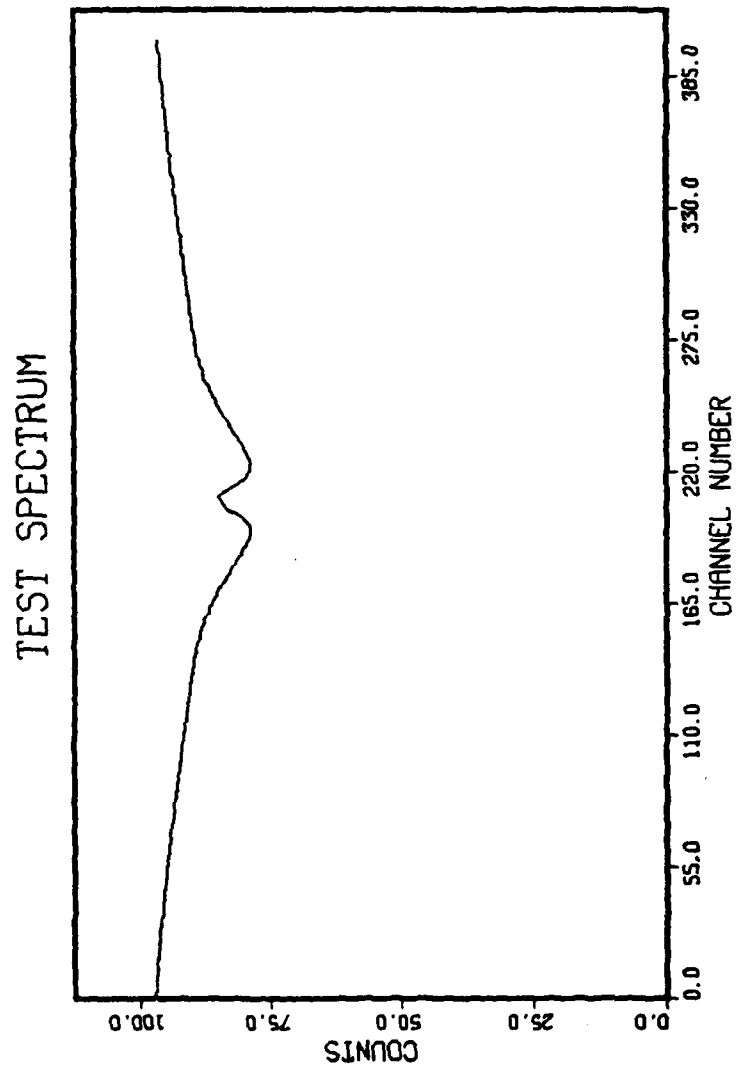


Figure 8. Input Test Spectrum

least-squares minimization in MOSFIT should be virtually identical to those in Figures 7 and 8. However, as evidenced by Figures 9 and 10, the plots do not correspond. The expansion coefficients for the magnetic field in Figure 9 were found to be

$$a_0 = 0.4842$$

$$a_2 = 0.0864$$

which are roughly one-half the value of the input coefficients $a_0 = 1$ and $a_2 = 0.1667$. Although the background count of ~102 counts does roughly correspond to the 100 counts of the input, it appears that a factor of two is missing somewhere in the program. Therefore, the expansion coefficients were multiplied by two and the program was run again. The results are shown in Figures 11 and 12. These results reproduce the general shape of $\rho(H)$ and the fit spectrum seems to match the test input rather well. In addition, the fit spectrum was determined using the $r_n(c)$ values rather than a numerical integration. An apparent discrepancy occurs in these runs. The fit spectrum found without multiplying the expansion coefficients by two follows the actual data more closely than the "corrected" spectrum. This can be seen in Figures 13 and 14. The magnetic field densities corresponding to these results are identical to those in Figures 9 and 11. Therefore, it is obvious that although the spectrum in Figure 13 appears to

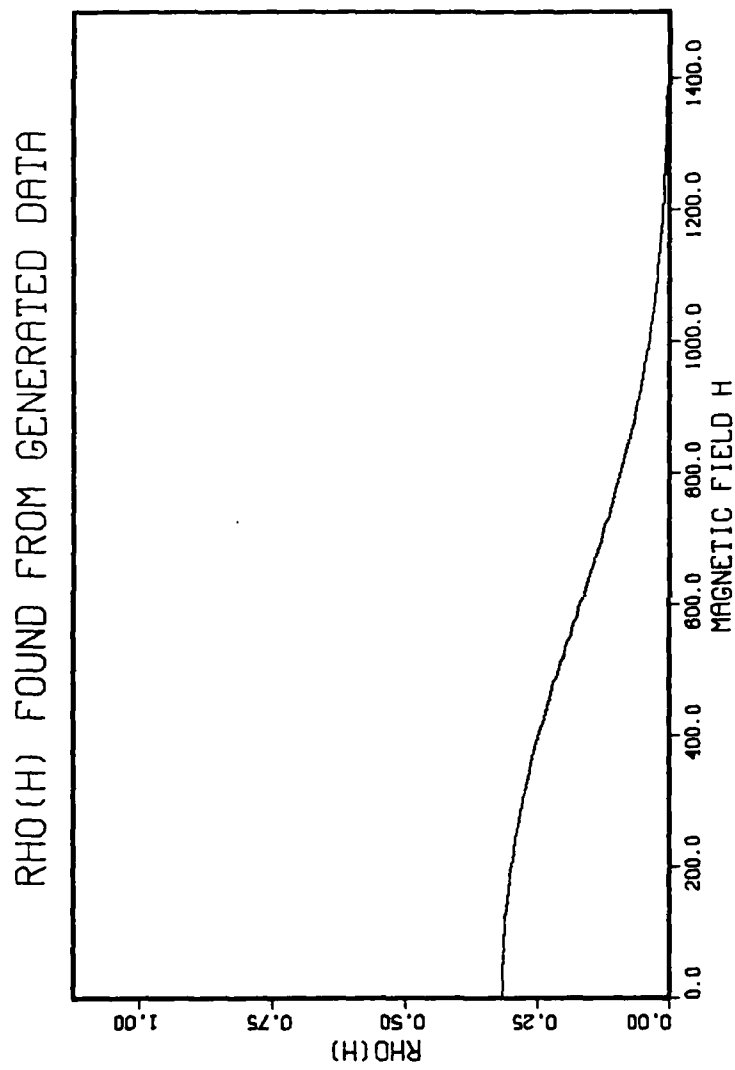


Figure 9. Magnetic Field Density from Initial Test Run

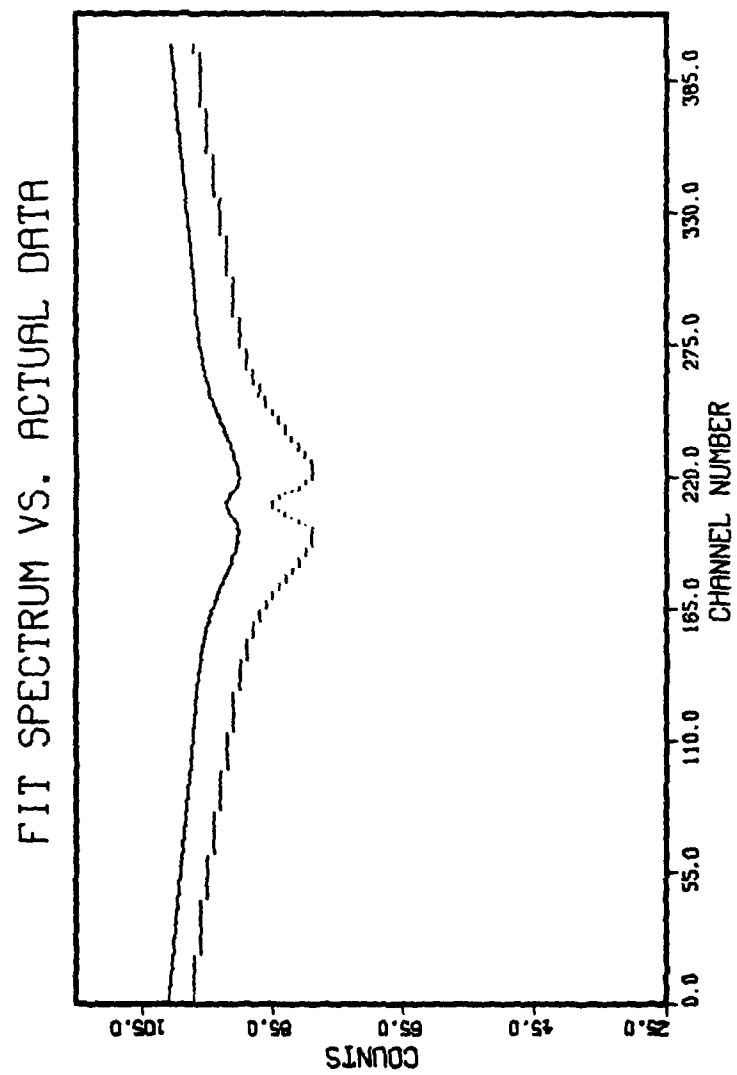


Figure 10. Fit Spectrum from Numerical Integration
in Initial Run

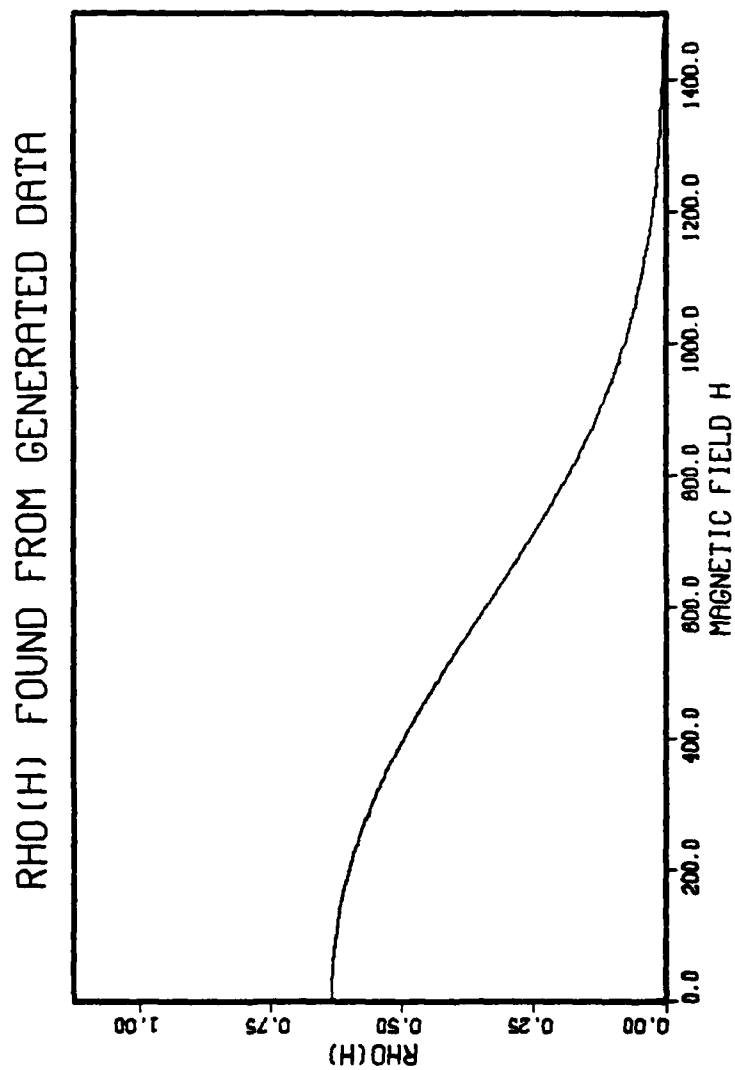


Figure 11. Magnetic Field Density With
2x Correction Factor

FIT SPECTRUM VS. ACTUAL DATA

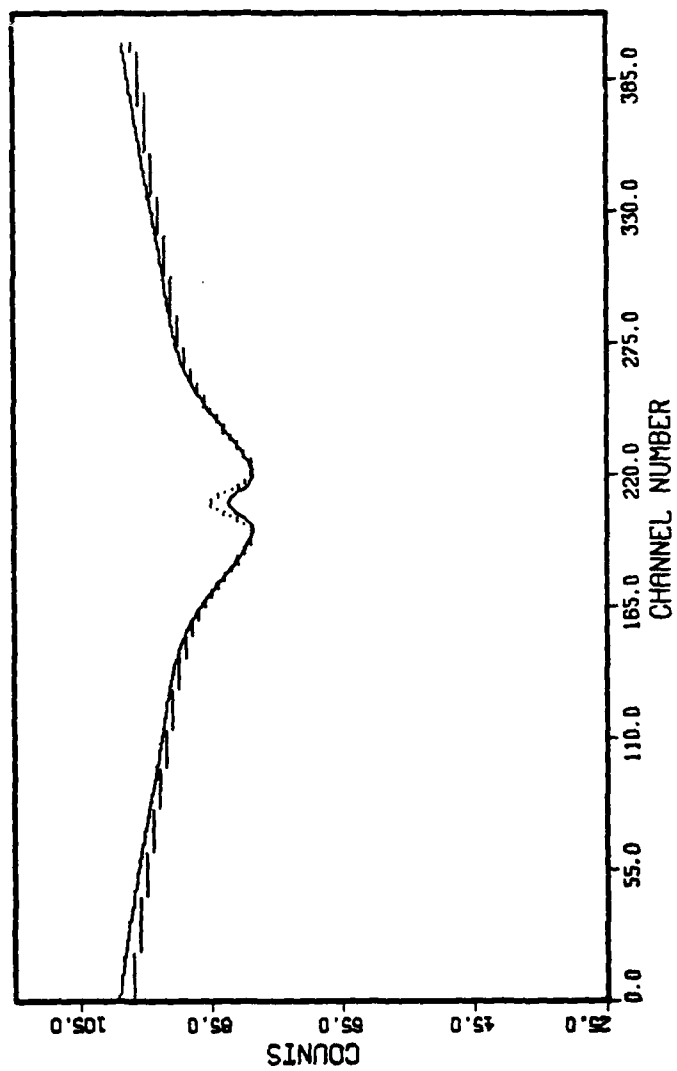


Figure 12. Fit Spectrum by Numerical Integration
and 2x Factor

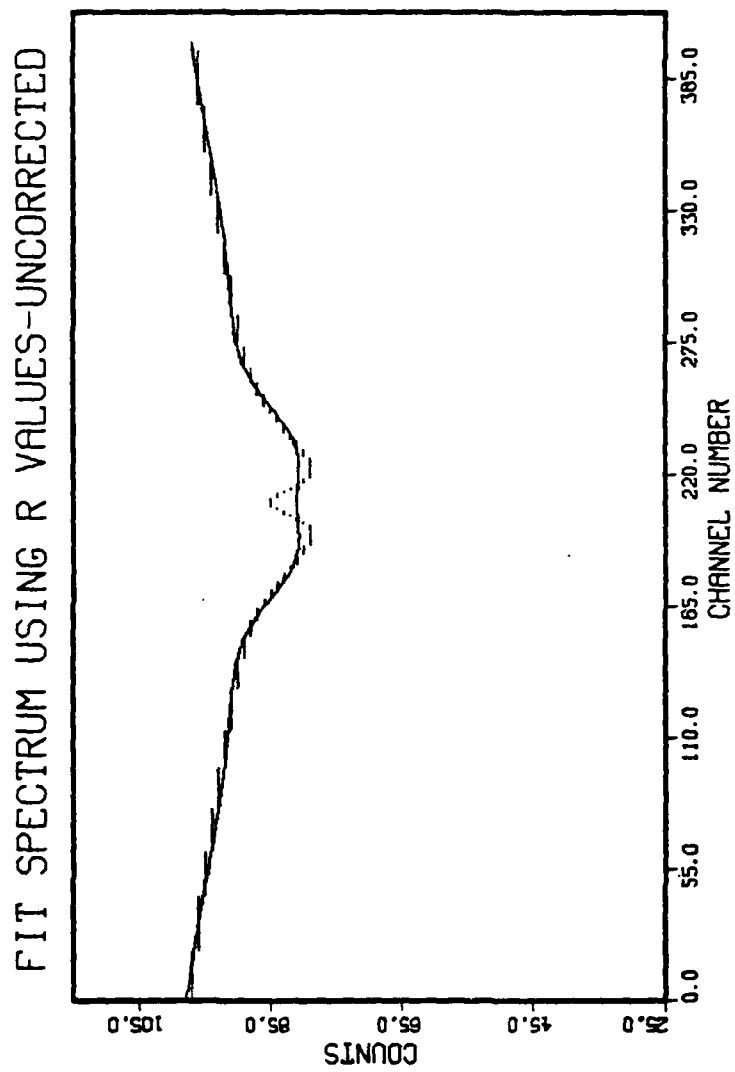


Figure 13. Fit Spectrum Using $r_n(c)$ Values
Without 2x Factor

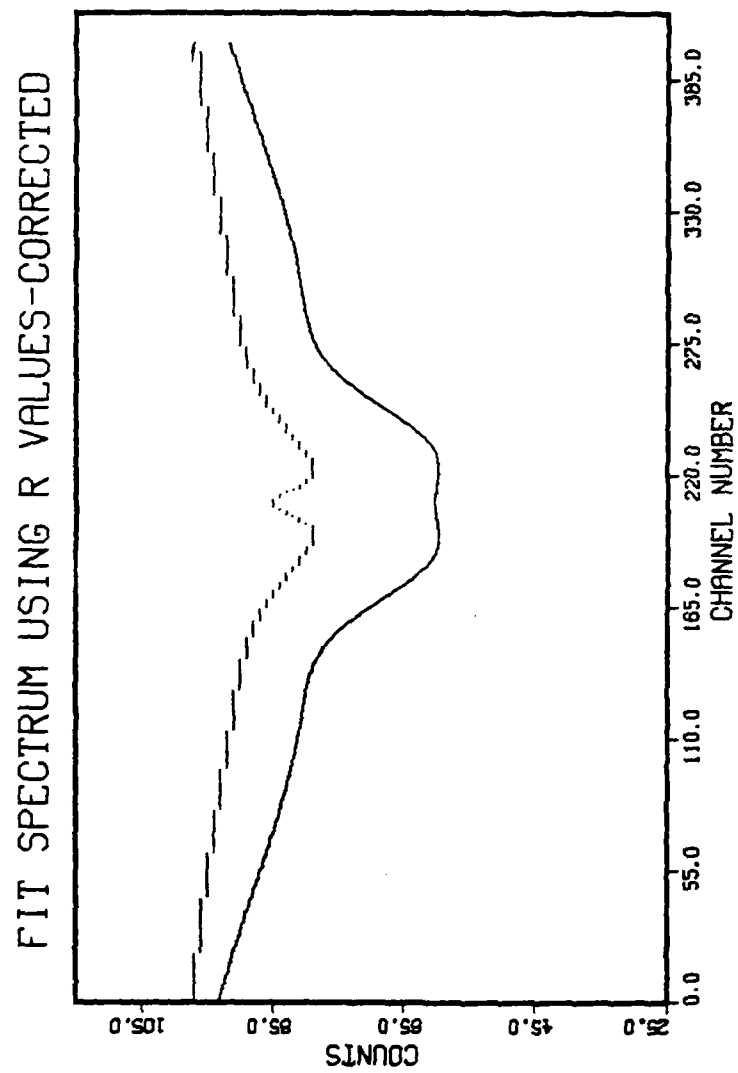


Figure 14. Fit Spectrum Using $r_n(c)$ Values
and 2x Factor

be a "good" fit, the corresponding magnetic field density does not match the input. These problems were not resolved.

V. Results, Recommendations and Conclusions

The objectives of this study have not been entirely met because of an unknown error(s) in the computer implementation of this theory. This chapter will examine the proposed optimization of the results in a fully operational program, conclusions drawn from the work done to this point, and recommendations for further study and modification.

Optimizing Results

It is obvious from Chapter IV that no reasonable results have been produced since no actual data has been processed. However, in the fitting of $\rho(H)$, the question arises as to the number of orthonormal functions ϕ_n required to "best-fit" the system. This problem is solved if the system S (Eq (2.12)) is evaluated after the minimization. That is, using the minimized parameters, a_n , b_γ , λ_q , find a value of S for the given number of polynomials n . The expected result of a plot of $\ln(s)$ versus n is shown in Figure 15. This figure shows that the value of S is expected to decrease with increasing n , then level off in a plateau region, followed by a sharp drop off at large n . The best fit is found with an n in the plateau region where S is at its minimum value. The region of sharp decrease in S after

the plateau is not useful because the fit begins to follow the actual data too closely beyond this point.

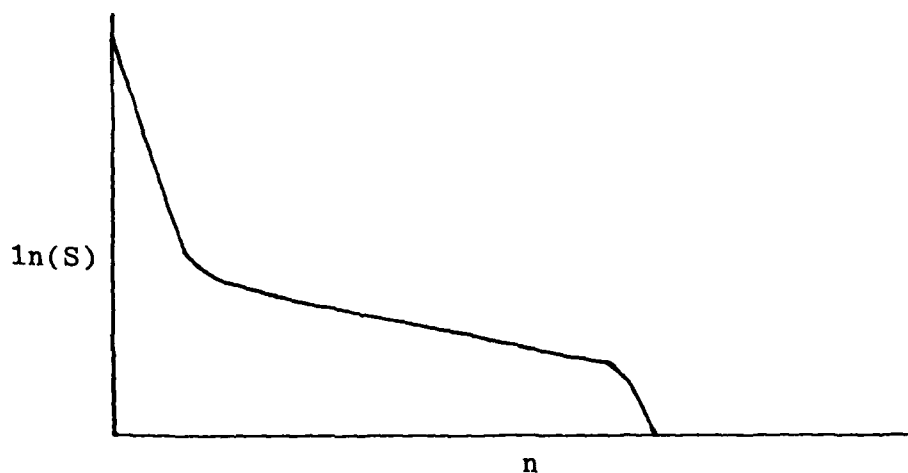


Figure 15. Result Optimization

Conclusions

The problem with the programming is not known; however, an error of a factor of two should be able to be found in a straightforward manner. First, in considering the actual input data (Figures 7 and 8), it was noted that the magnetic field density was calculated without the normalization constant $(\frac{1}{2^n n! \sqrt{\pi}})^2$ for H_0 . This constant has a value of approximately 0.75. Since the program MOSFIT uses the orthonormal functions ϕ_n in the expansion of $\rho(H)$, this is clearly one source of disagreement between input and results. The discrepancy that arises when the $r_n(c)$ values are used is more difficult to explain. These r values are computed with a factor of $(1./\sqrt{2})^n$. This factor

reduces the magnitude of the second order r terms by one-half. Obviously, if this factor is incorrect, another source of disagreement is found.

An interesting observation that has been made is that all odd r terms are zero and can be ignored in these calculations. This fact is intuitively obvious, based on the early assumption that the magnetic field density is symmetric about zero. In addition, with careful examination of Eq (2.35b) and the definition of the Hermit argument in Eq (2.43), it is easily shown that all $r_n(c)$ values must equal zero for odd n .

It is also significant to note that although Pate's velocity fit is dependent on specific data, it does not necessarily eliminate the data independent character of the $r_n(c)$ values. The velocity fit corresponds to an NFE spectrum, which is used as a "base spectrum" for the determination of the magnetic field density. Since this same base spectrum will be used each time, the velocity parameters do in fact become data independent. However, if a specific velocity/channel fit is desired for each set of data, this can be readily incorporated into the program. The multichannel analyzer that stores the counting data includes velocity data as well.

Finally, these results, although far from conclusive, appear to show that with minor corrections this program may provide a viable method to fit the magnetic field distribution from amorphous metal alloys.

Recommendations

The principal recommendation must be that this study be continued to conclusion with other parties investigating the theory and programming in order to find the minor error. Simple manipulation of the existing programs should ascertain if the two factors discussed earlier are contributors to the error. Obviously, the current programming should be modified to eliminate the computation and use of all odd $r_n(c)$ values, since all of these values are zero. In addition, an important change would be to find a better way to do channel to velocity conversion. If the entire programming could be redeveloped in relation to velocity rather than channel number, conversion routines would not be necessary and computation time would be enhanced. Also, in determining the fit spectrum, it is recommended that the $r_n(c)$ parameters be used instead of numerical integration routines. This will increase the speed and should improve the accuracy of the results.

Finally, any computational problems in the solution of the matrix problem may be overcome by using double precision numbers. However, with the large storage space

already in use, the longer turn-around time may negate any benefit gained. Another interesting facet would be to add a statistical Goodness of Fit test to the programming in order to test the final spectrum. Finally, once this program is fully operational, it would be interesting to examine its effectiveness on spectra of amorphous metal alloys since the programming was developed for this purpose and these materials have been of recent interest to the Air Force.

Bibliography

1. Goldanski, V.I. and R. H. Heber. Chemical Applications of Mössbauer Spectroscopy. New York: Academic Press, 1968.
2. Gonser, U. Mössbauer Spectroscopy. New York: Springer-Verlay, 1975.
3. -----. Professor of Physics, Air Force Institute of Technology (private communication). Wright-Patterson AFB, Ohio, July 1981.
4. McCullough, D. T. "Finding the Magnetic Field Distribution from Mossbauer Spectra." Unpublished MS thesis. Wright-Patterson AFB, Ohio, School of Engineering, Air Force Institute of Technology, March, 1981.
5. Phillips, D. L. "A Technique for the Numerical Solution of Certain Integral Equations of the First Kind." Journal of the Association for Computing Machinery, Vol. 9, No. 1, 84-97 (1962).
6. Le Caer, G. and J. M. Dubois. "Evaluation of Hyperfine Parameter Distributions from Overlapped Mössbauer Spectra of Amorphous Alloys." Journal of Physics E: Scientific Instruments, Vol. 12, 1083-90 (1979).
7. Window, B. "Hyperfine Field Distributions from Mössbauer Spectra." Journal of Physics E: Scientific Instruments, Vol. 4, 1401-2 (1971).
8. Hesse, J. and A. Rubartsch. "Model Independent Evaluation of Overlapped Mössbauer Spectra." Journal of Physics E: Scientific Instruments, Vol. 7, 526-32 (1978).
9. Vincze, I. "Evaluation of Complex Mossbauer Spectra in Amphorous and Crystalline Ferromagnetics." Solid State Communications, Vol. 25, 689-93 (1978).
10. Schmidt, T. A. "Analysis of Metallic Glasses by Mössbauer Spectroscopy." Unpublished MS thesis. Wright-Patterson AFB, Ohio, School of Engineering, Air Force Institute of Technology, March, 1978.
11. Guest, P. G. Numerical Methods of Curve Fitting. New York: Cambridge University Press, 1966.

12. Knoll, G. F. Radiation Detection and Measurement. New York: John Wiley and Sons, 1979.
13. Pate, B. E. "Development of a Minicomputer-Based Mössbauer Spectrometer." Unpublished MS thesis. Wright-Patterson AFB, Ohio, School of Engineering, Air Force Institute of Technology, March, 1982.
14. Hornbeck, R. W. Numerical Methods. New York: Quantum Publishers, Inc., 1975.
15. Hertz, W. C., ed. Program Test Methods. New Jersey: Prentice-Hall, Inc., 1973.

Appendix A

Input Parameters for Program RPARAM

Program RPARAM requires the input of certain parameters that describe the expected spectral shape. For example, note the relationship between these parameters and the spectrum in Figure A-1.

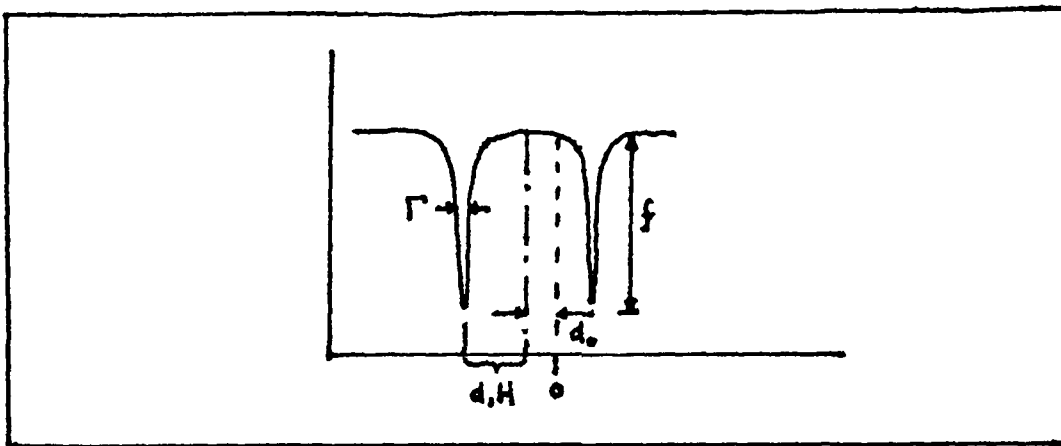


Figure A-1. Relation of Input Parameters to Spectrum

The purpose of this discussion is to direct the reader to the correct quantities in the literature for input into this program. Since the absorber in amorphous metal alloys is Fe^{57} , the quantities related to this isotope will be discussed here.

Two of the quantities, Γ and H_0 , are of a rather arbitrary nature. Gamma (Γ), which represents the spectral

linewidth can be taken as a quantity somewhat larger than the natural linewidth of the nucleus under investigation. This follows from the expected broadening of the peaks with respect to the natural linewidth. The linewidth was taken as .23 mm/sec based on previous work. The natural linewidth is found as .194 mm/sec in the literature (Ref 2). H_0 is an arbitrary scaling factor for the dimensionless variable Z . H_0 is chosen to give an appropriate distribution $\rho(Z)$. If H_0 is chosen too large, the distribution is spread over a wide range of field strength, while a smaller H_0 will narrow the distribution. The H_0 in this program was varied, but the best results seem to be found with $H_0 = 400$ kOe.

The f factor is not the recoil-free fraction found in the literature. Instead, f represents the relative intensity of each spectral peak. The calculated intensity of the individual components of a spectrum involves rather complex calculations and can be found in the literature (Ref 1). The relative intensities of the lines in the Fe^{57} spectrum integrated over all directions is found to be 3:2:1:1:2:3 (Ref 2).

Finally, the spreading quantities are best understood by examining the splitting of the Fe^{57} nucleus (Figure A-2).

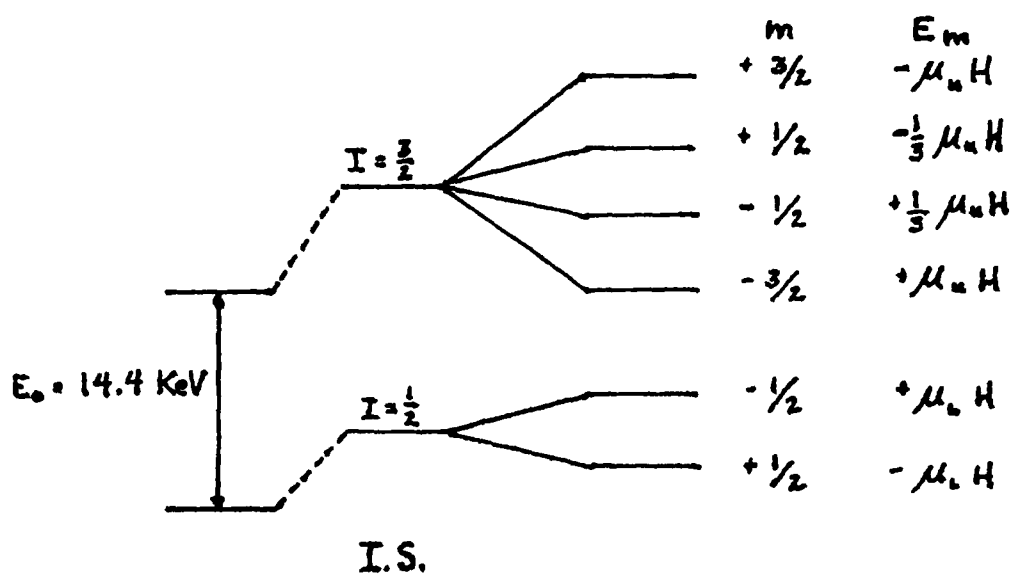


Figure A-2. Splitting of the Fe^{57} Nucleus

The energy eigenvalue of a given level m is found as

$$E_m = -g_N \beta_N H m_I \quad (\text{A-1})$$

where g_N is the nuclear Lande splitting factor, β_N is the nuclear Bohr magneton and m_I is the magnetic quantum number. However, the nuclear magnetic moment is

$$\mu = g_N \beta_N I \quad (\text{A-2})$$

and the energy eigenvalues are

$$E_m = \left(\frac{-\mu m_I}{I} \right) H \quad (\text{A-3})$$

which are evaluated in Figure A-2. The ΔE_m for a transition is found from the difference in E_m for the allowed transitions. Therefore, the energy of a gamma-ray is found as

$$E_{\gamma} = E_0 + \Delta E_m \quad (A-4)$$

The energy E_0 is perturbed by the isomer shift (I.S.) so that

$$E_{\gamma} = E_0 + \text{I.S.} + \Delta E_m \quad (A-5)$$

From Eq (A-5), it follows that d_0 and d_1 are found as

$$d_0 = E_0 + \text{I.S.}$$

$$d_1 = \Delta E_m / H$$

Since E_0 relates to a zero velocity, $d_0 = \text{I.S.}$, which gives the input to RPARAM, when the values of μ_u and μ_l are known. For Fe^{57} , $\mu_u = -.153\text{nm}$ and $\mu_l = +.0903\text{nm}$.

It is evident that there is flexibility in the definition of the d parameters discussed above. This study has only considered the magnetic field interactions in the Mossbauer analysis. If electric field or quadripole interactions are of importance, these effects could be included in the d terms.

Appendix B

Computer Program Listings

The computer programming for this problem was written in FORTRAN V for a CDC Cyber mainframe. Programs RPARAM and MOSFIT are discussed in detail in Chapter III and will not be examined here. However, it should be noted that MOSFIT does require the addition of one card for input data. The program determines constraints based on user input. All other data is entered in DATA statements. Also, plotting requires the DISSPLA package and online plotting capability. Program DATA is a modification of subroutine SPCTRM in MOSFIT and was used to generate data for program testing.

Flowcharts of selected subroutines are also included in this Appendix. Subroutines CONS, INTEG, COEFF, HERMIT, MAGFD and SPCTRM have been examined. The flowcharts for these routines will be found immediately following their individual listings.

The program listings that follow are numbered for ease in finding the subroutines. The index is as follows:

RPARAM

<u>Subroutine</u>	<u>Page</u>	<u>Line Number</u>
CONS	73	17
INTEG	75	33
RITEO	77	56
FIX	78	72

MOSFIT

<u>Subroutine</u>	<u>Page</u>	<u>Line Number</u>
READN	80	39
COEFF	81	61
MATR1	85	121
HERMIT	86	154
MAGFD	88	180
SMOOTH	90	203
PLTMAG	91	239
SPCTRM	92	260
PLTSPT	96	304

```

1=      PROGRAM RPARAM
2=      REAL A
3=      COMMON/CDP/D(16),CMA(6),F(6),DE,H8,P1
4=      COMMON/CDT/A(16),N(6,400),Z(6,400)
5=      COMMON/CDT/FNS(6,0:5,400),R(0:3,400)
6=      DIMENSION C(400)
7=      DATA K,L,M/6,9,400/
8=      DATA DE,D1/.26,-.2497,-.1419,-.0393,.0393,.1419,.2497/
9=      DATA CMA,H2/.23,.23,.23,.23,.23,.23,436./
10=     DATA F,P1/3,.2,.1,.1,.2,.3,.3,1415927/
11=     CALL FIX(K)
12=     CALL CONS(K,M)
13=     CALL INTEG(K,L,M)
14=     CALL RITE0(L,M)
15=     STOP
16=     END

```

Copy available to DTIC does not
 permit fully legible reproduction

```

17=      SUBROUTINE CONG(K,M)
18=      INTEGER CI
19=      REAL NVAL,NO
20=      COMMON/DTA/D1(6),DTT(4,6),F(6),Z0,-B,F1
21=      COMMON/CON/A(6),N(6,400),Z(6,400)
22=      DO 10 J=1,K
23=      A(J)=SQRT((D1(J)*-B)**2-G**A(J)**2)/((D1(J)*-B)**2+G**A(J)**2)
24=      NO=B/1PI**((1./4.)*SQRT(G**A(J)**2+D1(J)**2*-B**2))
25=      DO 20 CI=1,M
26=      NX=EXP(-101-D3)**2/(2.*(G**A(J)**2+D1(J)**2*-B**2))
27=      Z(J,CI)=D1(J)*-B*(20-CI)/SQRT((D1(J)*-B)**2-G**A(J)**2)
28=      N(J,CI)=NO*NX
29=20      CONTINUE
30=10      CONTINUE
31=      RETURN
32=      END

```

Copy available to DTIC does not
 permit fully legible reproduction

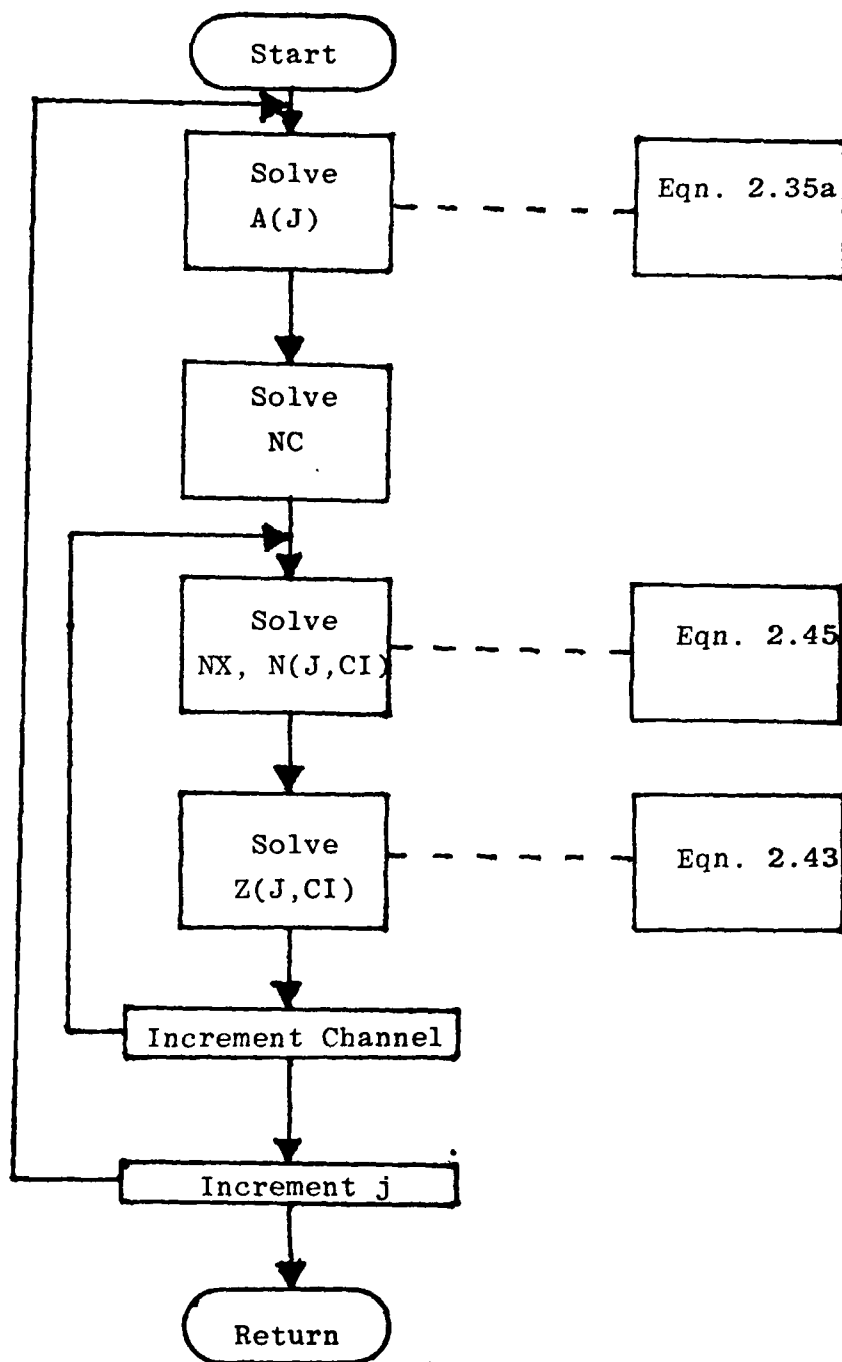


Figure B-1. Flowchart for Subroutine CONS

```

33=      SUBROUTINE INTEG(M,L,N)
34=      INTEGER S,CI
35=      REAL A
36=      COMMON/DTA/D1(6),DMMA(3),F(6),E3,E2,P1
37=      COMMON/CON/A(6),N(6,422),Z(6,422)
38=      COMMON/OUT/FN(6,6,5,422),R(2,3,422)
39=      DO 38 S=0,L
40=      S1=S
41=      DO 40 CI=1,M
42=      P(S,CI)=0.
43=      DO 50 J=1,K
44=      FN(J,3,CI)=N(J,CI)
45=      FN(J,4,CI)=Z(J,CI)*A(J)*Z(J,4,CI)
46=      IF (E3.EQ.0) THEN
47=      FN(J,5,CI)=(Z(J,CI)/SQRT(S+1.))* (Z(J,CI)+FN(J,3,CI)-A(J)
48=      : *FN(J,4,CI)*SQRT(S1))
49=      ENDIF
50=      R(S,CI)=F(J)*(1./SQRT(2.))*S)*FN(J,5,CI)+R(S,CI)
51=53      CONTINUE
52=40      CONTINUE
53=32      CONTINUE
54=      RETURN
55=      END

```

Copy available to DTIC does not
 permit fully legible reproduction

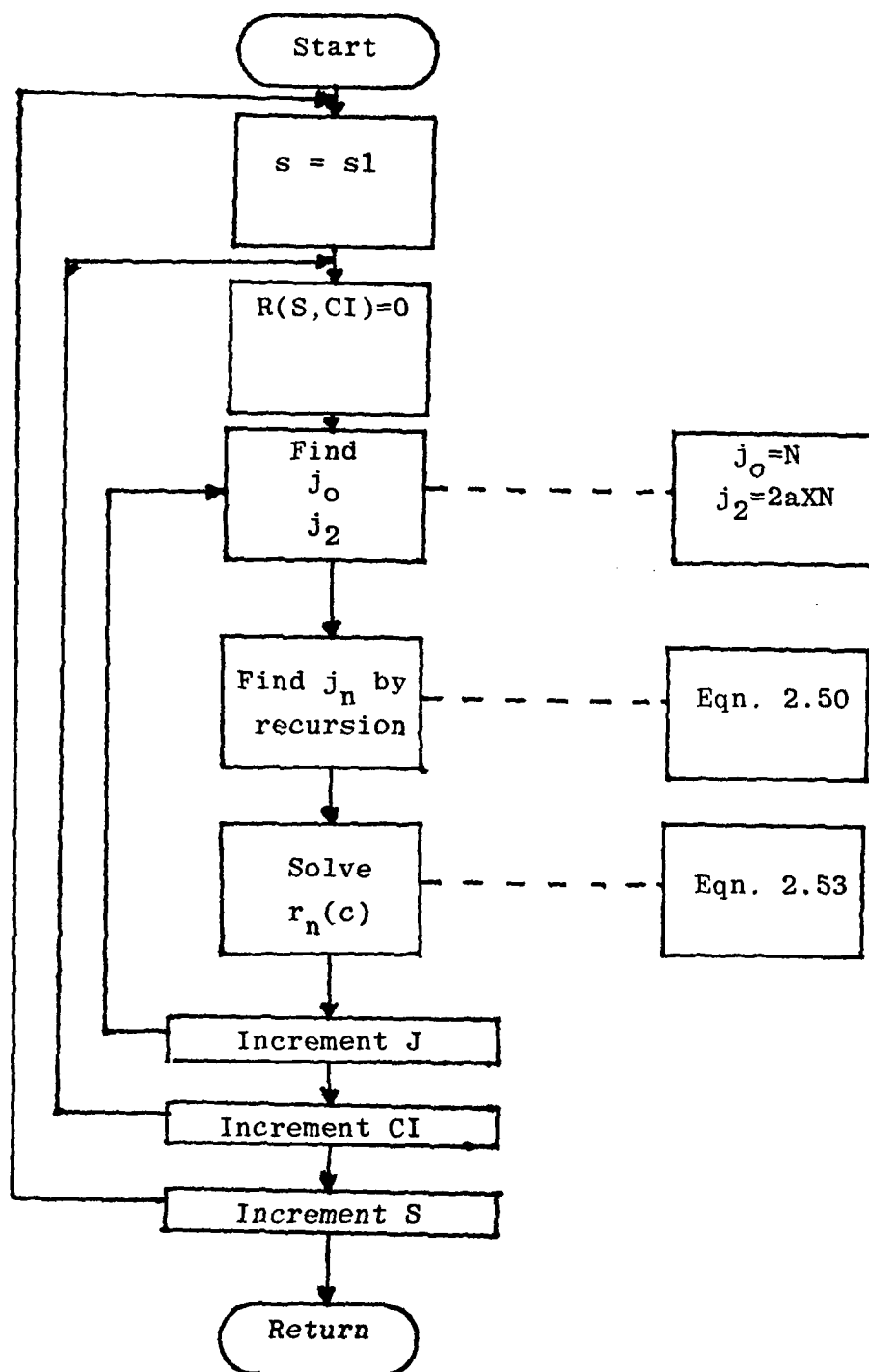


Figure B-2. Flowchart for Subroutine INTEG

```

56=      SUBROUTINE RITER(L,P)
57=      INTEGER S,C1
58=      COMMON/OUT/FNJ(16,0:5,400),R(0:3,400)
59=      DO 60 C1=1,M
60=      NN=0
61=100    IF(NN,LE,L) THEN
62=      WRITE(9,1000) (R(S,C1),S=NN,NN+3)
63=      NN=NN+5
64=      GOTO 100
65=      ELSE
66=      GOTO 60
67=      ENDIF
68=60    CONTINUE
69=1000  FORMAT(4E14.7)
70=      RETURN
71=      END

```

Copy available to DTIC does
 permit fully legible reproduction


```

72=      SUBROUTINE F1X(M)
73=      COMMON/DT/D1(8),GMM(8),F1(8),D0(8),F1
74=      DATA EG,GMMSEC/14.4125,2.997925E11/
75=      DATA CONV/3.1574417E-12/
76=      DO 10 J=1,M
77=          D1(J)=CONV*D1(J)*GMMSEC/EG
78=          D1(J)=D1(J)/.84819964
79=          GMM(J)=GMM(J)/.84819964
80=10      CONTINUE
81=      T8=(D0+9.795998)/.84819964
82=      RETURN
83=      END

```

Copy available to DTIC does not
 permit fully legible reproduction

```

1= PROGRAM M05FIT
2= REAL N
3= CHARACTER CONSTRA1
4= COMMON/INDEX/K,L,M
5= COMMON/MATED/E(4,4),E(4,3),E(3,3),P(4),G(3)
6= COMMON/INPT/R(8:9,400),X(400)
7= COMMON/HERM/HF(2:102,0:5),H(0:100),RHO(0:100),H0,DELH
8= COMMON/DRVE/F(6),D1(6),RL(400),CYMA(6),DB
9= DIMENSION BD(15),A(15,15),Y(15)
10= DATA K,L,M/7,9,400/
11= DATA NA/15/
12= NN=1
13= READ(*,1000) CONSTR
14=C
15=C          READ STATEMENT TESTS FOR ADDITION OF CONSTRAINTS.
16=C          1 ON CARD - NO CONSTRAINTS.
17=C
18= CALL READN
19= CALL COEFF
20= CALL MATR1(A,Y,NA)
21= CALL HERMIT
22= IF (CONSTR.EQ.'0') GOTO 100
23= CALL CONST
24= CALL MATRN
25=100 CALL MESCHF(A,NA,K,Y,NA,1,IE,DB)
26=C
27=C          SUBROUTINE MESCHF IS A ROUTINE WRITTEN BY DR SHANKLAND T
28=C          PERFORM A CHOLESKY DECOMPOSITION FOR THE SOLUTION OF THE
29=C          MATRIX PROBLEM. IT REQUIRES EINDEK=1, ID=7768142 TO B
30=C          ATTACHED AS A LIBRARY.
31=C
32= CALL MAGFD(Y,NA)
33= CALL SPCTRM(Y,NA)
34= CALL PLTMAG(NN)
35= CALL PLTSPT(NN)
36=1000 FORMAT(A1)
37= STOP
38= END

```

```

39=      SUBROUTINE READN
42=      REAL N
41=      INTEGER S,CI
42=      COMMON/INCK/K,L,M
43=      COMMON/INPT/R(0:3,400),N(400)
44=C
45=C      THIS SUBROUTINE READS IN THE RAW DATA AS
46=C      WELL AS THE R PARAMETER PREVIOUSLY COMPUTED
47=C      AND STORED. DATA FILE IS ATTACHED AS TAPE8
48=C      AND R IS TAPE9.
49=C
50=      DO 10 I=1,M/10
51=      READ(8,1000) KK,(N(CI),CI=KK+1,KK+10)
52=10      CONTINUE
53=      DO 20 CI=1,M
54=      NN=0
55=      READ(9,1100) (R(CI),S=NN,NN+3)
56=20      CONTINUE
57=1000    FORMAT(10,10F7.0)
58=1100    FORMAT(4E14.7)
59=      RETURN
60=      END

```

```

61= SUBROUTINE COEFF
62= REAL N
63= INTEGER S,CI,GMA,SS,GMA1
64= COMMON/INDX/K,L,M
65= COMMON/INPT/R(2:3,400),N(400)
66= COMMON/MATCO/D(4,4),E(4,3),P(4),Q(3)
67= DIMENSION AA(4)
68= DATA H3,IR,A/400,12,1./
69= C      EACH SET OF MATRIX COEFFICIENTS IS CALCULATED
70= C      IN THIS SUBROUTINE.
71= C
72= DO 10 GMA=0,2
73= G(GMA+1)=0.
74= DO 15 CI=1,M
75= G(GMA+1)=N(CI)*2*CI*GMA+G(GMA+1)
76=15 CONTINUE
77=10 CONTINUE
78= DO 20 S=0,L
79= P(S+1)=0.
80= DO 25 CI=1,M
81= P(S+1)=N(CI)*2*R(S,CI)+P(S+1)
82=25 CONTINUE
83=20 CONTINUE
84= DO 30 GMA=0,2
85= DO 32 S=0,L
86= D(S+1,GMA+1)=0.
87= DO 35 CI=1,M
88= D(S+1,GMA+1)=N(CI)*R(S,CI)+CI*GMA+D(S+1,GMA+1)
89=35 CONTINUE
90=32 CONTINUE
91=30 CONTINUE
92= DO 40 S=0,L
93= DO 50 SS=0,L
94= B(S+1,SS+1)=0.
95= DO 60 CI=1,M
96= B(S+1,SS+1)=N(CI)*R(S,CI)*R(SS,CI)+B(S+1,SS+1)
97=60 CONTINUE
98= IF (S.NE.SS) THEN
99= RB=0.

```

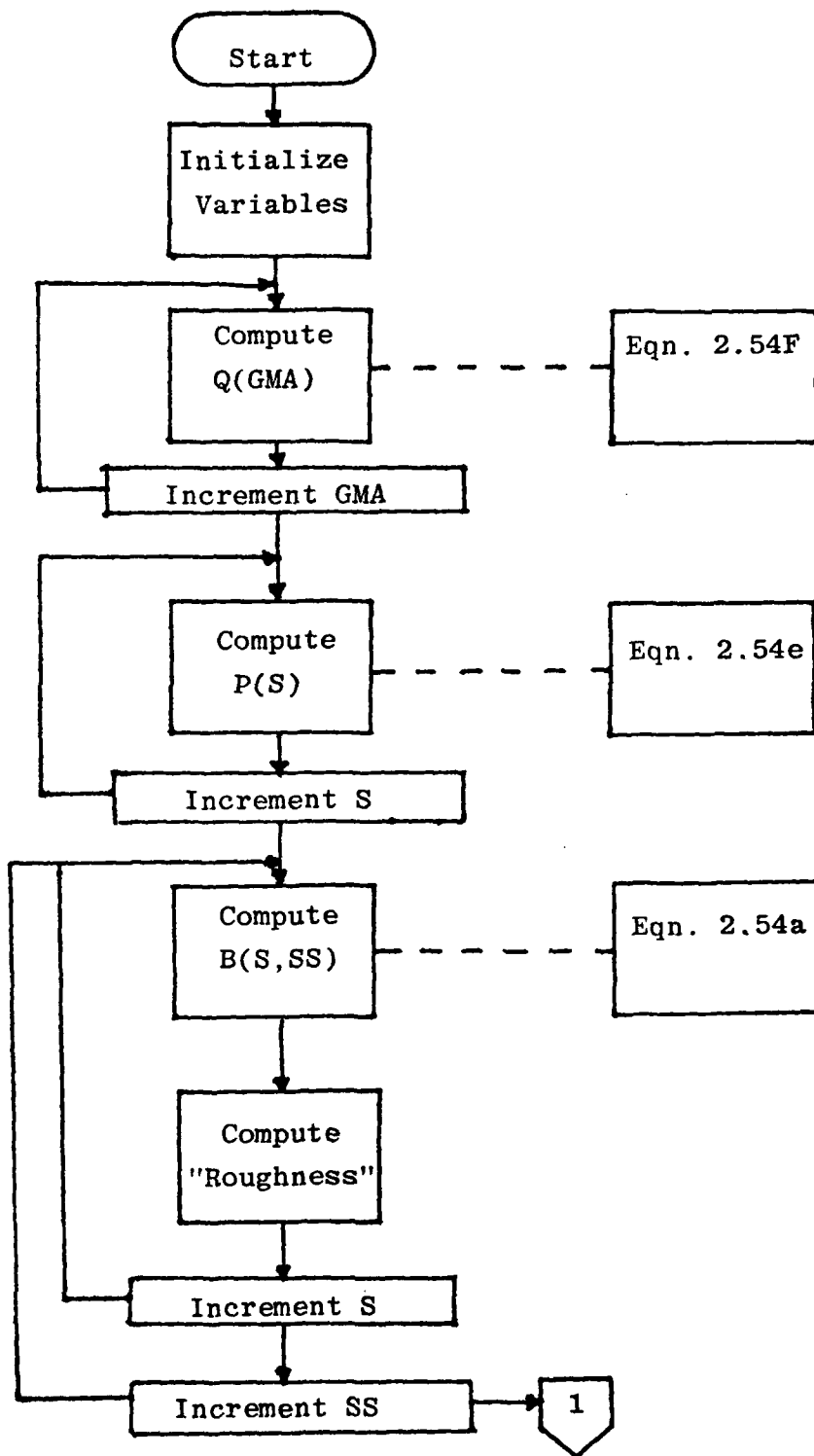


Figure B-3. Flowchart for Subroutine COEFF

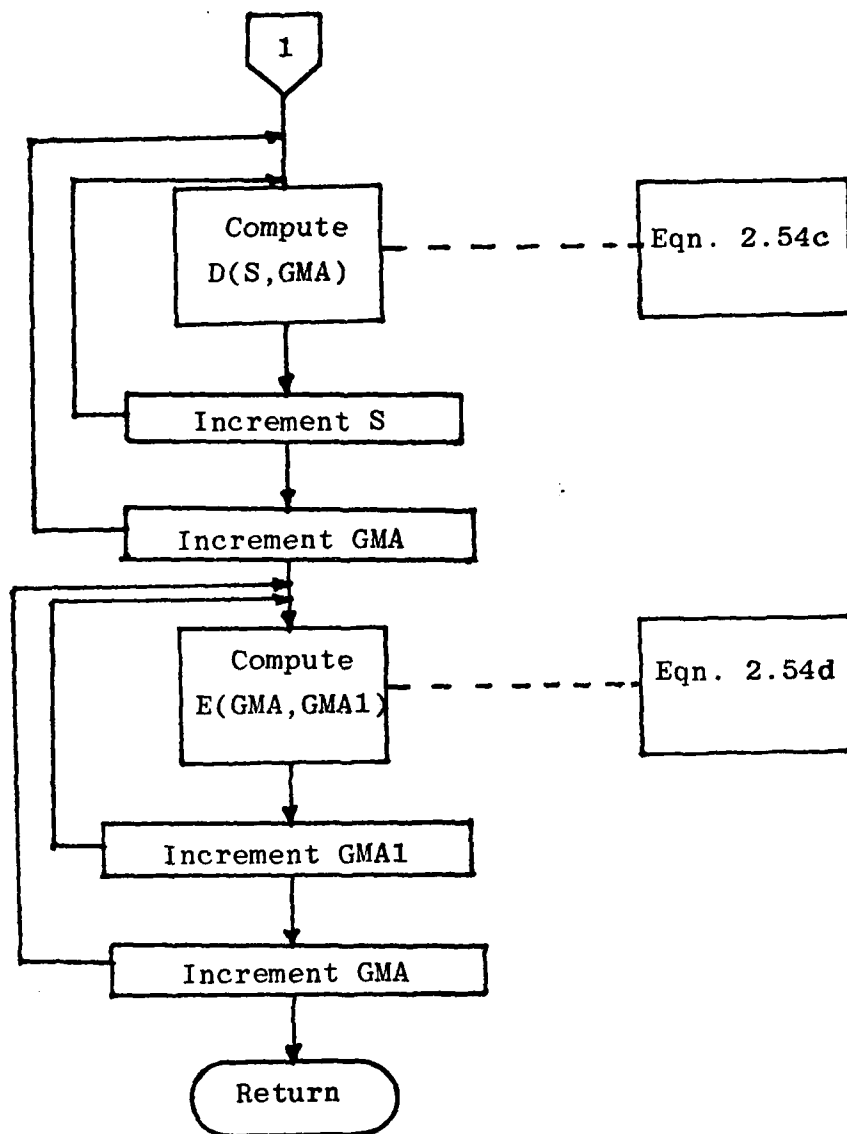


Figure B-4. Continuation of COEFF Flowchart

```

100=      ELSE
101=      RZ=Z.
102=      DO 65 I=1,IR
103=      AA(I)=EXP(-(S+.5)/(2.*I))**2)
104=      RZ=AA(I)*(1+(S+.5)**2)**I+RZ
105=65    CONTINUE
106=      RZ=A*H2*RZ
107=      ENDIF
108=      B(S+1,SS+1)=B(S+1,SS+1)+RZ
109=50    CONTINUE
110=40    CONTINUE
111=      DO 70 GMA=0,2
112=      DO 80 GMA1=0,2
113=      E(GMA+1,GMA1+1)=0.
114=      DO 50 CI=1,7
115=      E(GMA+1,GMA1+1)=N(CI)*CI** (GMA+GMA1)+E(GMA+1,GMA1+1)
116=92    CONTINUE
117=80    CONTINUE
118=70    CONTINUE
119=      RETURN
120=      END

```

```

121= SUBROUTINE MATR1(A,Y,NA)
122= COMMON/MATC3/D(4,4),D(4,3),E(3,3),P(4),Q(3)
123= COMMON/INQ1/K,L,M
124= DIMENSION A(NA*NA),Y(NA)
125=
126= THIS SUBROUTINE ADDS THE INDIVIDUAL MATRIX
127= COEFFICIENTS TO THE MATRIX A. THIS OPERATION
128= COULD BE INCORPORATED INTO SUBROUTINE COEFF.
129=
130= DO 10 I=1,L+1
131= DO 20 J=1,L+1
132= A(I,J)=D(I,J)
133=12 CONTINUE
134=10 CONTINUE
135= DO 30 I=1,L+1
136= DO 40 J=1,3
137= A(I,J+L+1)=-D(I,J)
138= A(J+L+1,I)=-D(I,J)
139=40 CONTINUE
140=30 CONTINUE
141= DO 50 I=1,3
142= DO 60 J=1,3
143= A(I+L-1,J+L+1)=E(I,J)
144=60 CONTINUE
145=50 CONTINUE
146= DO 70 I=1,L+1
147= Y(I)=-P(I)
148=70 CONTINUE
149= DO 80 I=1,3
150= Y(I+L+1)=Q(I)
151=80 CONTINUE
152= RETURN
153= END

```



```

154=      SUBROUTINE HERMIT
155=      INTEGER S
156=      COMMON/INDEX/M,L,N
157=      COMMON/HERM/HP(2:100,0:5),H(0:100),RHO(2:100),HE,DELH
158=      DATA H2,DELH/400.,.15./
159=
160=      SUBROUTINE HERMIT GENERATES THE HERMIT POLY-
161=      NOMIALS ACCORDING TO THE RECURSION RELATION
162=       $HN+1(X) = 2 * X * HN(X) - 2 * N * H - 1(X)$ .
163=
164=      DO 10 I=0,100
165=      IF (I.EQ.0) THEN
166=      H(I)=0.
167=      ELSE
168=      H(I)=H(I-1)*DELH
169=      ENDIF
170=      DO 20 S=0,L
171=      HP(I,S)=1.
172=      HP(I,1)=2.*H(I)/H0
173=      IF (S.GT.2) THEN
174=      HP(I,S+1)=2.*(H(I)/H2)*HP(I,S)-2.*S*HP(I,S-1)
175=      ENDIF
176=20    CONTINUE
177=10    CONTINUE
178=      RETURN
179=      END

```

AD-A115 483

AIR FORCE INST OF TECH WRIGHT-PATTERSON AFB OH SCH00--ETC F/6 12/1
SMOOTH FIT ANALYSIS OF MOESSBAUER SPECTRA.(U)

MAR 82 T L BAZZOLI

AFIT/GNE/PH/82-2

NL

UNCLASSIFIED

2 of 2

AD A
1 0483



END
DATE
FILMED
DTIC
0782

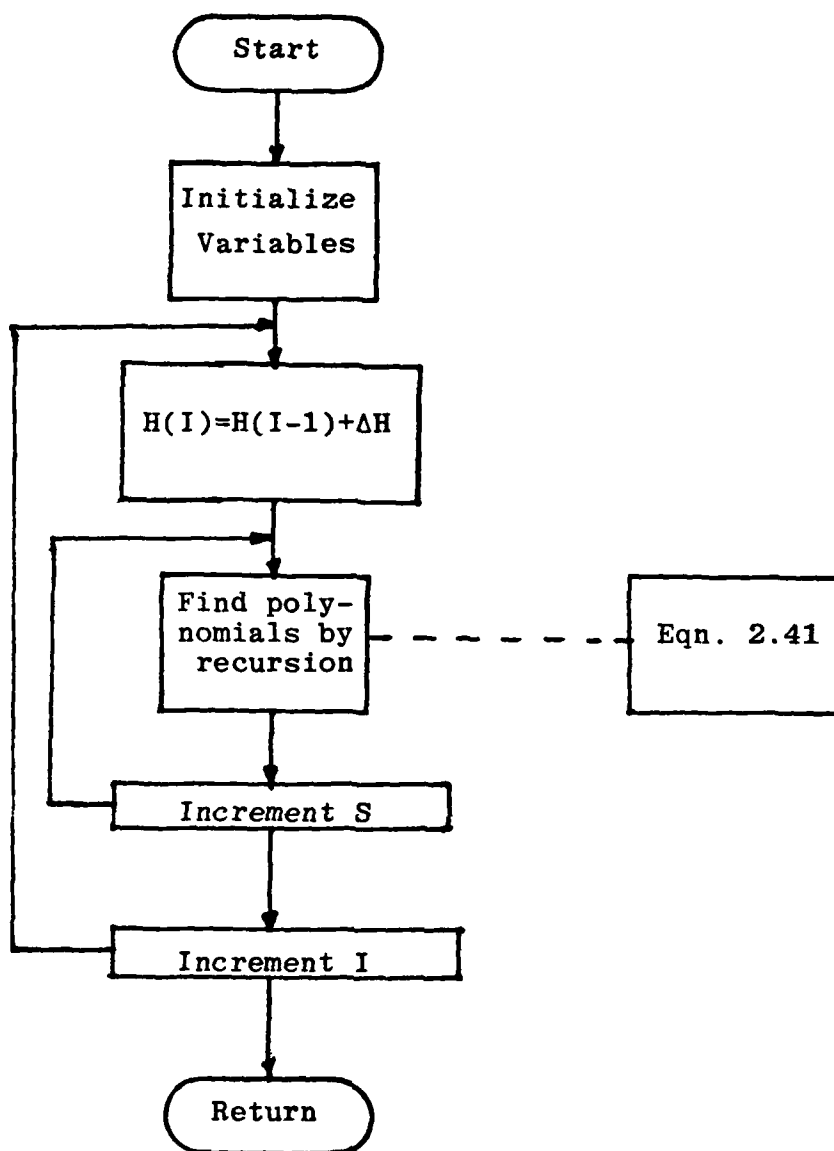


Figure B-5. Flowchart for Subroutine HERMIT

```

182= SUBROUTINE MAGFB(Y,NA)
181= INTEGER S
182= COMMON/INDEX/K,L,M
183= COMMON/HERM/HP(0:100,0:5),H(0:100),RHO(0:100),H0,DELH
184= DIMENSION Y(NA)
185= DATA PI/3.1415927/
186=C
187=C          THIS SUBROUTINE USES PREVIOUSLY GENERATED
188=C          HERMITE POLYNOMIALS WITH THE MATRIX SOLUTION Y
189=C          TO DETERMINE THE MAGNETIC FIELD DENSITY.
190=C
191= DO 10 I=0,100
192=   RHO(I)=0.
193=   FACT=1.
194=   CORTH=EXP(-((X(I)-H0)/H0)**2)/2.)
195=   DO 20 S=0,L
196=     CNORM=SQRT(1./((2.**S*PI**5*FACT)))
197=     R-D(I)=CNORM*CORTH**Y(S+1)*HP(I,S)+RHO(I)
198=     FACT=FACT*(S+1)
199=20   CONTINUE
200=10   CONTINUE
201=   RETURN
202=   END

```

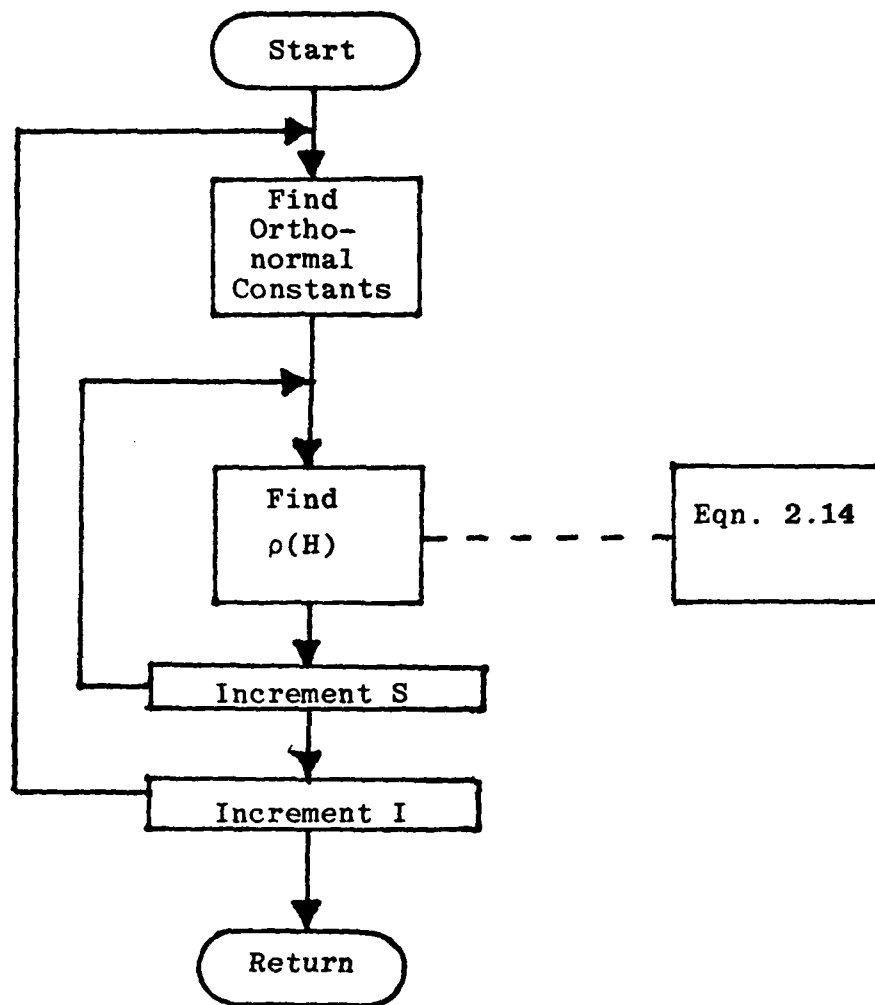


Figure B-6. Flowchart for Subroutine MAGFD

```

223=      SUBROUTINE SMOOTH(Y,NA)
224=      INTEGER S,CI
225=      COMMON/INDEX/K,L,M
226=      COMMON/INFT/R(B:3,400),N(400)
227=      DIMENSION Y(NA),C(2,2)
228=      DATA A/1./
229=      SUM2=0.
230=      DO 10 CI=1,M
231=          SUM1=0.
232=          DO 20 S=0,L
233=              SUM1=Y(S)*R(S,CI)+SUM1
234=20      CONTINUE
235=          SUM2=N(CI)*(N(CI)-Y(L+2)-Y(L+3)*CI-Y(L+4)*CI**2+SUM1)
236=          : **2+SUM2
237=10      CONTINUE
238=          CONST=0.
239=          DO 30 NQ=1,Q
240=              NL=L+4
241=              DO 40 S=0,L
242=                  CONST=Y(NL+NQ)*Y(S)+C(S,NQ)+CONST
243=40      CONTINUE
244=30      CONTINUE
245=          ROUGH=0.
246=          DO 50 S=0,L
247=              DO 60 SS=0,L
248=                  IF (S.NE.SS) COTO 60
249=                  DO 70 I=1,IR
250=                      AA=EXP(-((S+.5)/(2.*I))**2)
251=                      RO=AA*(1+(S+.5)**2)**I+RO
252=70      CONTINUE
253=          ROUGH=NQ*Y(S)**2*RO+ROUGH
254=60      CONTINUE
255=50      CONTINUE
256=          FIT=.5*SUM1-CONST+A*ROUGH
257=          RETURN
258=          END

```

```

239= SUBROUTINE PLT*AC(NN)
240= COMMON/HER*/HP(0:120,0:5),H(0:100),RHO(0:100),H0,DELH
241= COMMON/INDX/K,L,M
242=C
243=C      THIS SUBROUTINE USES THE DISPLA PACKAGE
244=C      TO PLOT THE MAGNETIC FIELD DENSITY AS A
245=C      FUNCTION OF H. THE DISPLA PKG MUST BE
246=C      ATTACHED AS A LIBRARY TO USE THIS ROUTINE.
247=C
248= CALL COMPS
249= CALL BONPL(NN)
250= CALL GRACE(0,1)
251= CALL TITLE('RHO(H) FOUND FROM GENERATED DATA',-100,
252= 'MAGNETIC FIELD H',100,'RHO(H)',100,7.5,4.5)
253= CALL GRAPH(0,230,0,25)
254= CALL CURVE(H,RHO,100,0)
255= CALL FRAME
256= CALL ENPL(NN)
257= NN=NN+1
258= RETURN
259= END

```

```

260=      SUBROUTINE SFOTR*(Y,NA)
261=      COMMON/HER*/H(0:100,0:5),H(0:100),RHD(0:100),H0,DELH
262=      COMMON/INDEX/K,L,M
263=      COMMON/CRVE/F(6),D1(6),RL(400),GMMA(6),D0
264=      DIMENSION Y(NA),BKGRND(400)
265=      DATA GMMA,D0,PI/.20,.20,.20,.20,.20,.20,3.1415927/
266=      DATA F,D1/D0,.2,.1,.1,.2,.3,-.2437,-.1413,-.0393,.0393,
267=      :.1413,.2437/
268=      DATA KK/6./
269=C
270=C      THIS SUBROUTINE DETERMINES THE FID SPECTRUM
271=C      FROM THE PREVIOUSLY COMPUTED MAGNETIC FIELD
272=C      DENSITY USING THE BACKGROUND - FID MODEL.
273=C
274=      CALL FIX(KK,D0,D1,GMMA)
275=      DO 10 I=1,M
276=      BKGRND(I)=Y(L+2)+Y(L+3)*I-Y(L+4)*I**2
277=      RL(I)=0.
278=      DO 25 IK=1,KK
279=      DO 27 J=1,100
280=      EX=(-(1-D0-(D1(IK)+H(J)))*2/(2.*GMMA(IK)**2))
281=      IF (EX.LT.-250.) THEN
282=      RL(I)=RL(I)+0.
283=      ELSE
284=      RL(I)=F(IK)*EXP(EX)/(GMMA(IK)*SQRT(2.*PI))*DELH*RHD(J)+RL(I)
285=      ENDIF
286=27      CONTINUE
287=25      CONTINUE
288=      RL(I)=BKGRND(I)-RL(I)
289=10      CONTINUE
290=      RETURN
291=      END

```

Copy available to DTIC does not
 permit fully legible reproduction /


```

260= SUBROUTINE SPOTRM(Y,NA)
261= COMMON/HERT/H(0:100,0:5),H1(0:100),RH0(0:100),H0*DELH
262= COMMON/INX/K,KL,M
263= COMMON/CRVE/F(4),D(10),RL(400),GMMA(6),D0
264= COMMON/IAPT/R(0:3,400),N(400)
265= DIMENSION Y(NA),BKGRND(400)
266= DATA GMMA,D0,F1/.20,.20,.20,.20,.20,.20/.3,1415927/
267= DATA F,D1/3,.2,.1,.1,.2,.3,,-.2437,-.1413,-.0093,.0093,
268= :.1413,.2437/
269= DATA KK/6./
270=C
271=C
272=C THIS SUBROUTINE DETERMINES THE FIT SPECTRUM
273=C FROM THE PREVIOUSLY COMPUTED MAGNETIC FIELD
274=C DENSITY USING THE BACKGROUND AS MODELLED.
275=C THIS VERSION OF SPOTRM USES THE F(5:6)
276=C VALUES IN PLACE OF A NUMERICAL INTEGRATION.
277= CALL FIX(KK,D0,D1,GMMA)
278= DO 10 I=1,M
279= BKGRND(I)=Y(L+2)+Y(L+3)*I+Y(L+4)*I**2
280= RL(I)=0.
281= DO 25 J=0,L
282= RL(I)=Y(J+1)*R(J,I)+RL(I)
283=25 CONTINUE
284= RL(I)=BKGRND(I)-RL(I)
285=10 CONTINUE
286= RETURN
287= END

```

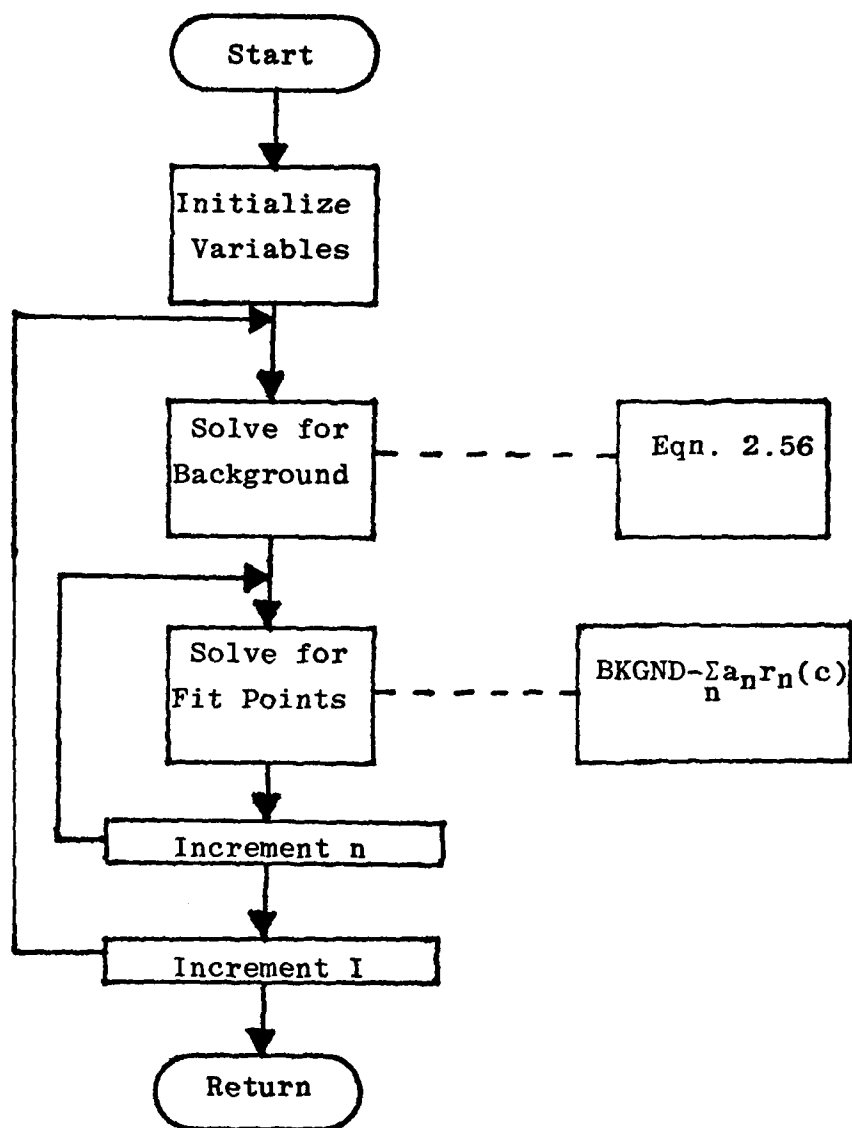


Figure B-7. Flowchart for Subroutine SPCTRM

```

292= SUBROUTINE FIX(K,D2,D1,GMA)
293= DIMENSION D1(K),GMA(K)
294= DATA ES,GMMSEC/14.4125,2.997925E11/
295= DATA CONV/3.1574417E-12/
296= DO 10 J=1,K
297=   D1(J)=CONV*D1(J)*GMMSEC/ES
298=   D1(J)=D1(J)/.04819964
299=   GMA(J)=GMA(J)/.04819964
300=10 CONTINUE
301=   D2=(D2+9.795998)/.04819964
302= RETURN
303= END

```

Copy available to DTIC does not
 permit fully legible reproduction /

```

304=      SUBROUTINE PLTSPT(NN)
305=      REAL N
306=      COMMON/INPT/R(0:3,400),N(400)
307=      COMMON/CRVE/F(6),D1(6),RL(400),GMMA(6),L3
308=      DIMENSION C(400)
309=      DO 20 K=1,400
310=      C(K)=K
311=20     CONTINUE
312=      CALL EGNPL(NN)
313=      CALL TITLE('FIT SPECTRUM VS. ACTUAL DATA$',-100,'CHANNEL NUMBERS',
314=      :100,'COUNTS$',100,7.5,4.5)
315=      CALL GRAPH(2,55,25,20.)
316=      CALL CURVE(C,RL,400,2)
317=      CALL MARKER(1)
318=      CALL SCLPIC(.001)
319=      CALL CURVE(C,N,400,-1)
320=      CALL RESET('SCLPIC')
321=      CALL GRACE(.31)
322=      CALL FRAME
323=      CALL ENDPL(NN)
324=      CALL DONEPL
325=      RETURN
326=      END

```

```

1= PROGRAM DATA
2= REAL N
3= DIMENSION H(0:100),RHO(1:20),RL(400),N(400)
4= DIMENSION F(6),C(400),D1(6),GMA(6)
5= DATA GMA,D0,P1/.20,.20,.20,.20,.20,.20,.20,.1415927/
6= DATA F,D1/0.,2.,1.,1.,2.,0.,-.2437,-.1415,-.0393,.0393,
7= .1415,.2437/
8= DATA H0,H0,DELH/1,400,.15./
9= KK=6
10= A=1./6.
11= H(0)=0.
12= BKORND=100.
13= DO 20 J=1,100
14= H(J)=H(J-1)+DELH
15= CH0=(1./SQRT(F1))**.5
16= CH2=(1./((2.*2*2.*SQRT(F1))**.5
17= H0=4.*(H(0)/H0)**2-2.
18= RHO(J)=EXP(-(H(J)-H0)**2/2.)*(1.-RHO+RHO-2*CH0)
19=20 CONTINUE
20= LL=0
21= DO 30 J=1,20
22= WRITE(9,1100) LL,(RHO(J),JJ=LL+1,LL+5)
23= LL=LL+5
24=30 CONTINUE
25= CALL F1N(K,C,D1,GMA)
26= DO 10 I=1,400
27= RL(I)=0.
28= DO 25 IK=1,KK
29= DO 27 J=1,100
30= EX=(-(1.-C0-((21(IK)+H(J))**2/(2.*GMA(IK)**2))
31= IF (EX.LT.-250.) THEN
32= RL(I)=RL(I)+0.
33= ELSE
34= RL(I)=F(IK)*EXP(EX)/(GMA(IK)*SQRT(2.*PI))*DELH*RHO(J)+RL(I)
35= ENDIF
36=27 CONTINUE
37=25 CONTINUE
38= RL(I)=BKORND-RL(I)
39=10 CONTINUE

```

```
40=      KK=0
41=      DO 40 I=1,40
42=      WRITE(10,1000) KK,(RL(I),I=KK+1,KK+10)
43=      KK=KK+10
44=40    CONTINUE
45=1000  FORMAT(10,10F7.0)
46=1100  FORMAT(10,5F14.0)
47=      STOP
48=      END
```

Vita

Thomas Lynn Bazzoli was born 31 January 1958 in Camden, New Jersey. He graduated from John Dickinson High School in Wilmington, Delaware in June 1976 and received the Bachelor of Science degree in Chemistry from The Citadel, The Military College of South Carolina in May 1980. Upon graduation, he was commissioned in the United States Air Force through the ROTC program. He entered active duty in June 1980 as a resident graduate student at the Air Force Institute of Technology at Wright-Patterson AFB, Ohio.

Permanent address: 1208 McKennan's Church Road
Wilmington, Delaware 19808

UNCLASSIFIED

SECURITY CLASSIFICATION OF THIS PAGE (When Data Entered)

REPORT DOCUMENTATION PAGE		READ INSTRUCTIONS BEFORE COMPLETING FORM
1. REPORT NUMBER AFIT/GNE/PH/82-2	2. GOVT ACCESSION NO. AD-A115483	3. RECIPIENT'S CATALOG NUMBER
4. TITLE (and Subtitle) SMOOTH FIT ANALYSIS OF MOSSBAUER SPECTRA		5. TYPE OF REPORT & PERIOD COVERED MS Thesis
7. AUTHOR(s) Thomas L. Bazzoli Lieutenant		6. PERFORMING ORG. REPORT NUMBER
9. PERFORMING ORGANIZATION NAME AND ADDRESS Air Force Institute of Technology (AFIT-EN) Wright-Patterson AFB, Ohio 45433		8. CONTRACT OR GRANT NUMBER(s)
11. CONTROLLING OFFICE NAME AND ADDRESS		10. PROGRAM ELEMENT, PROJECT, TASK AREA & WORK UNIT NUMBERS
14. MONITORING AGENCY NAME & ADDRESS (if different from Controlling Office)		12. REPORT DATE March, 1982
		13. NUMBER OF PAGES 100
		15. SECURITY CLASS. (of this report) UNCLASSIFIED
		15a. DECLASSIFICATION/DOWNGRADING SCHEDULE
16. DISTRIBUTION STATEMENT (of this Report) Approved for public release; distribution unlimited.		
17. DISTRIBUTION STATEMENT (of the abstract entered in Block 20, if different from Report) 15 APR 1982		
18. SUPPLEMENTARY NOTES APPROVED FOR PUBLICATION AFR 190-17. Dean for Research and Professional Development Air Force Institute of Technology (ATC) Wright-Patterson AFB, OH 45433		
19. KEY WORDS (Continue on reverse side if necessary and identify by block number) Mossbauer Amorphous Magnetic Field Curve Fitting		
20. ABSTRACT (Continue on reverse side if necessary and identify by block number) A method of fitting the magnetic field distribution from Mossbauer spectra using a linear least-squares technique was proposed where the distribution is assumed to be an expansion in Hermite polynomials. This method was developed, programmed and tested on a test spectrum with a known distribution of magnetic field. The programming was not entirely successful in reproducing this test spectra and no actual data was analyzed to support the effectiveness of this method.		

DD FORM 1473

JAN 73

EDITION OF 1 NOV 65 IS OBSOLETE

UNCLASSIFIED

SECURITY CLASSIFICATION OF THIS PAGE (When Data Entered)

**DAT
FILM**

7-8